ISSN 0915-633X

NATIONAL INSTITUTE FOR FUSION SCIENCE

Effects of Finite-β and Radial Electric Fields on Neoclassical Transport in the Large Helical Device

R. Kanno, N. Nakajima, H. Sugama, M. Okamoto and Y. Ogawa

(Received - Dec. 18, 1996)

NIFS-472 Jan. 1997

RESEARCH REPORT
NIFS Series

NAGOYA, JAPAN

Effects of finite-β and radial electric fields on neoclassical transport in the Large Helical Device

R. KANNO, N. NAKAJIMA, H. SUGAMA, M. OKAMOTO

National Institute for Fusion Science,

Nagoya, Japan

Y. OGAWA

Department of Quantum Engineering and System Science,

Faculty of Engineering,

University of Tokyo,

Tokyo, Japan

ABSTRACT. Effects of finite-β and radial electric fields on the neoclassical transport in the Large Helical Device are investigated with the DKES (Drift Kinetic Equation Solver) code. In the finite-β configuration, even orbits of deeply trapped particles deviate significantly from magnetic flux surfaces. Thus, neoclassical ripple transport coefficients in the finite-β configuration are several times larger than those in the vacuum configuration under the same condition of temperatures and radial electric fields. When the plasma temperature is several keV, a bifurcation of the electric fields appears under the ambipolarity condition, and sufficient large radial electric fields can be generated. As a result, the $\boldsymbol{E} \times \boldsymbol{B}$ drift rectifies orbits of particles and improves significantly the transport coefficients in the finite-β configuration.

Keywords. neoclassical transport, LHD finite-β configuration, improvement by $\boldsymbol{E} \times \boldsymbol{B}$ drift, bifurcation of electric fields, DKES code.

1. Introduction

It is important to theoretically investigate neoclassical particle and energy confinement performances to design a reactor-grade collisionless plasma with good confinement performances and to understand transport phenomena in experiments.

From the viewpoint of the magnetohydrodynamic stability, helical configurations, *e.g.* the Large Helical Device (LHD) [1], have an advantage that in principle there does not exist a current driven instability such as in tokamaks. Here, the LHD is the pole number $L_{\rm p} = 2$ heliotron/torsatron type helical machine with superconducting coils of the pitch number $M_{\rm p} = 10$, and the configuration can be constructed by only external coils. On the other hand, the configuration has strong helical ripple components of the magnetic field, thus a geometrical symmetry disappears. For the plasma with a weak collisionality, trapped particles in the helical ripples mainly contribute to the diffusion of the plasma. As a result, the ripple transport dominates the confinement performances. This means that the transport coefficients are proportional to $1/\nu$, where ν is the collision frequency. However, if in the plasma there exists an electrostatic potential difference which is the same order of or larger than the plasma temperature, the $\boldsymbol{E}\times\boldsymbol{B}$ drift rectifies the orbits. From this effect, the transport coefficients can be improved significantly.

It is not easy to analyze quantitatively the neoclassical transport in realistic-systems because of complexity of the three-dimensional (3-D) magnetic field configuration without a symmetry. Hirshman et al. [2] have developed a powerful tool to analyze the neoclassical transport by solving the drift kinetic equation for plasmas with 3-D toroidal geometries. The tool is called the DKES (Drift Kinetic Equation Solver) code. This code is able to analyze the neoclassical transport under large radial electric fields. By using this code, several studies have been done to investigate the neoclassical transport in 3-D realistic-systems [2, 3, 4, 5]. For the LHD vacuum configuration, Ogawa et al. have estimated the neoclassical transport with the DKES code [5]. They calculated the thermal diffusivities only for the LHD vacuum configuration and studied the effect of multi-helicity of the magnetic field on the neoclassical transport coefficients.

In this paper, we study the neoclassical transport in the LHD finite-β configuration, especially noticing effects of finite-β and radial electric fields. As effects of finite-β, drift surfaces of particles deviate significantly from magnetic flux surfaces, thus we have to take into account the finite-β. And when we investigate effects of electric fields, radial electric fields have to be given by the ambipolarity condition. In the previous study by Ogawa et al. [5], they neglected effects of finite-β and used electric fields given *apriori* to estimate improvements of the confinements by the $\boldsymbol{E} \times \boldsymbol{B}$ drift. To more carefully investigate the confinement performances, we take into account both effects of finite-β and radial electric fields given by the ambipolarity condition. Furthermore, it is necessary to study effects of positions of the vacuum magnetic axis, because the confinement performances can be improved significantly by moving the vacuum magnetic axis inward [6, 5].

We select four configurations; the standard configurations $\Delta_{\rm v} = -0.15$ [m] with $\beta_0 = 0\%$ and 6%, and the inward-shifted configurations $\Delta_{\rm v} = -0.25$ [m] with $\beta_0 = 0\%$ and 8%, where β_0 is the beta-value at the magnetic axis and $\Delta_{\rm v}$ is the shift of the position of the vacuum magnetic axis which is measured from the major radius of helical coils $R_0 = 3.9$ [m]. Note that the vacuum magnetic axis can move horizontally from $R = 3.9$ [m] to 3.6 [m] in the vacuum. This movement corresponds to changing $\Delta_{\rm v}$ from 0 to -0.3 [m]. To investigate the neoclassical transport coefficients by using the DKES code, we need to obtain the Fourier spectrum of the magnetic field strength B in the Boozer coordinates. We apply the 3-D equilibrium code VMEC [7, 8] to the LHD with the central magnetic field $B_0 = 3$ [T] under the fixed boundary condition and with the assumption of the pressure profile $P = P_0(1 - \Phi_{\rm normal})^2$ and no net toroidal current, where $\Phi_{\rm normal} \equiv \Phi_{\rm T}/\Phi_{\rm T}^{\rm edge}$ is the normalized toroidal flux, $\Phi_{\rm T}$ is the toroidal flux, and $\Phi_{\rm T}^{\rm edge}$ is the value of the toroidal flux at the edge. We use the parameter $\Delta_{\rm v}$ to label the configuration, although the actual position of the magnetic axis in the finite-β configuration moves from $\Delta_{\rm v}$ to an outer position by the Shafranov shift [9].

In Section 2, we review briefly the method of calculation of the transport coeffi-

cients with the DKES code, following to Refs. [2, 3]. And the transport in the LHD configuration is interpreted by analytical results of Refs. [10, 11]. In Section 3, we calculate the transport coefficient under the ambipolarity condition, and try to understand qualitatively their behavior. And the transport under several additional conditions is investigated. The results are summarized in Section 4.

2. Transport analysis with the DKES code

2.1. Linearized drift kinetic equation solved by the DKES code

First of all, following to Refs. [2, 3], we review briefly the method of calculation of the transport coefficients by the DKES code. We can expand a distribution function of α-species-particle $f_\alpha(\boldsymbol{x}, \boldsymbol{v})$ around a local Maxwellian distribution $f_{\rm M}^\alpha = [n_\alpha/(\pi {v_{\rm th}^\alpha}^2)^{3/2}] \exp\{-K_\alpha\}$ as follows:

$$f_\alpha = f_{\rm M}^\alpha + f_1^\alpha, \tag{1}$$

where α denotes the species of charged particles, *i.e.* $\alpha = $ i for ions (hydrogens in this paper) and $\alpha =$ e for electrons. Here, f_1^α is the perturbation, $\boldsymbol{x} = (\rho, \theta, \zeta)$ denotes a position in the Boozer coordinates ($\rho = \Phi_{\rm T}/2\pi$), $\boldsymbol{v} = (v, \xi, \varphi)$ is a velocity in the spherical velocity-space coordinates, a density n_α and a temperature T_α are constant on a magnetic flux surface labeled by ρ, $v_{\rm th}^\alpha = \sqrt{2T_\alpha/m_\alpha}$ is the local thermal velocity, m_α is the mass, and $K_\alpha = (v/v_{\rm th}^\alpha)^2$ is the normalized kinetic energy. Under the Boozer coordinates (ρ, θ, ζ) the magnetic field is represented as

$$\boldsymbol{B} = \nabla\rho \times \nabla\theta - \iota \nabla\rho \times \nabla\zeta, \tag{2}$$

where ι is the rotational transform. Following to Refs. [2, 3], we consider the linearized drift kinetic equation:

$$V(f_1^\alpha) - C(f_1^\alpha) = D_\alpha, \tag{3}$$

where

$$V(f_1^\alpha) \;=\; \boldsymbol{v}_{\rm L} \cdot \nabla f_1^\alpha + \dot{\xi}_{\rm L} \frac{\partial f_1^\alpha}{\partial \xi}, \tag{4a}$$

$$\boldsymbol{v}_{\rm L} = v\cos\xi\boldsymbol{b} + E_\rho\frac{\nabla\rho\times\boldsymbol{B}}{\langle B^2\rangle}, \tag{4b}$$

$$\dot{\xi}_{\rm L} = -\frac{1}{2}v\sin\xi\boldsymbol{B}\cdot\nabla\left(\frac{1}{B}\right), \tag{4c}$$

$$C(f_1^\alpha) = \frac{1}{2}\nu\frac{\partial}{\partial\cos\xi}\left(\sin^2\xi\frac{\partial f_1^\alpha}{\partial\cos\xi}\right), \tag{4d}$$

$$D_\alpha = [-\boldsymbol{v}_{\rm D}^\alpha\cdot\nabla\rho(A_1^\alpha + K_\alpha A_2^\alpha) - Bv\cos\xi A_3^\alpha]\, f_{\rm M}^\alpha, \tag{4e}$$

$$\boldsymbol{v}_{\rm D}^\alpha = \frac{1}{m_\alpha\Omega_\alpha}\left[e_\alpha\boldsymbol{E} - \left\{\frac{m_\alpha(v\sin\xi)^2}{2}\right\}\nabla\ln B\right]\times\boldsymbol{b} + [\nabla\times\boldsymbol{b} - (\boldsymbol{b}\cdot\nabla\times\boldsymbol{b})\boldsymbol{b}]\frac{(v\cos\xi)^2}{\Omega_\alpha}, \tag{4f}$$

$$A_1^\alpha = \frac{{\rm d}\ln n_\alpha}{{\rm d}\rho} - \frac{3}{2}\frac{{\rm d}\ln T_\alpha}{{\rm d}\rho} - \frac{e_\alpha E_\rho}{T_\alpha}, \tag{4g}$$

$$A_2^\alpha = \frac{{\rm d}\ln T_\alpha}{{\rm d}\rho}, \tag{4h}$$

$$A_3^\alpha = -\frac{e_\alpha}{T_\alpha}\frac{\langle\boldsymbol{E}\cdot\boldsymbol{B}\rangle}{\langle B^2\rangle}, \tag{4i}$$

and $\boldsymbol{b} = \boldsymbol{B}/B$ is the unit vector in the direction of the magnetic field, E_ρ is the radial electric field, $\Omega_\alpha = e_\alpha B/m_\alpha$ is the cyclotron frequency, e_α is the charge. Here $\langle\cdots\rangle$ is the flux-surface-average operator defined as

$$\langle\cdots\rangle \equiv \frac{\int\int{\rm d}\theta{\rm d}\zeta\cdots\sqrt{\rm g}}{\int\int{\rm d}\theta{\rm d}\zeta\ \sqrt{\rm g}}, \tag{5}$$

where $\sqrt{\rm g} = (\nabla\rho\cdot\nabla\theta\times\nabla\zeta)^{-1}$ is the Jacobian.

Using the DKES code which solves Eq. (3) based on the variational principle, we can calculate the transport coefficients. Here the variational function, *i.e.* the entropy production rate $\dot{S}_\alpha$, is given by

$$\dot{S}_\alpha = \dot{S}_0^\alpha + \dot{S}_*^\alpha, \tag{6}$$

where

$$\dot{S}_0^\alpha = 2\left\{F_\alpha^+, \hat{V}(F_\alpha^-)\right\} - \left\{F_\alpha^+, \hat{C}(F_\alpha^+)\right\} + \left\{F_\alpha^-, \hat{C}(F_\alpha^-)\right\} - \left\{F_\alpha^+, D_\alpha\right\}, \tag{7a}$$

$$\dot{S}_*^\alpha = -\left\{F_\alpha^+, D_\alpha\right\}. \tag{7b}$$

Here $F_\alpha^\pm$ is defined by $F_\alpha^\pm \equiv (g_1^\alpha \pm h_1^\alpha)/2$; $g_1^\alpha \equiv f_1^\alpha/f_{\rm M}^\alpha$ and $h_1^\alpha(\cos\xi, E_\rho) = g_1^\alpha(-\cos\xi, -E_\rho)$ are perturbed distributions, operators $\hat{V}$ and $\hat{C}$ are defined as $\hat{V}(g_1^\alpha) \equiv f_{\rm M}^\alpha V(g_1^\alpha)$ and

$\hat{C}(g_1^\alpha) \equiv C(f_M^\alpha g_1^\alpha)$. The inner product $\{X, Y\}$ is defined by

$$\{X, Y\} \equiv 2\pi \int \mathrm{d}(\cos\xi) \int \mathrm{d}v\ v^2 \langle XY \rangle . \tag{8}$$

Note that $\dot{S}_*^\alpha$ is a stationary value of $\dot{S}_\alpha$. The second term in the right hand side of Eq. (6) can be described by using the thermodynamic fluxes I_j^α and the forces A_j^α:

$$\dot{S}_*^\alpha = -\{g_1^\alpha, D_\alpha\} = \sum_{j=1}^{3} I_j^\alpha A_j^\alpha, \tag{9}$$

where the fluxes I_j^α are represented as the product of the transport coefficients L_{jk}^α and the forces A_k^α;

$$I_1^\alpha \equiv \langle \boldsymbol{\Gamma}_\alpha \cdot \nabla\rho \rangle = -\sum_{k=1}^{3} n_\alpha L_{1k}^\alpha A_k^\alpha, \tag{10a}$$

$$I_2^\alpha \equiv \left\langle \frac{\boldsymbol{Q}_\alpha \cdot \nabla\rho}{T_\alpha} \right\rangle = -\sum_{k=1}^{3} n_\alpha L_{2k}^\alpha A_k^\alpha. \tag{10b}$$

$$I_3^\alpha \equiv n_\alpha \langle \boldsymbol{u} \cdot \boldsymbol{B} \rangle = -\sum_{k=1}^{3} n_\alpha L_{3k}^\alpha A_k^\alpha. \tag{10c}$$

Here, $\boldsymbol{\Gamma}_\alpha = \int \mathrm{d}^3v\, \boldsymbol{v}_\mathrm{D}^\alpha f_1^\alpha$ is the particle flux, $\boldsymbol{Q}_\alpha = T_\alpha \int \mathrm{d}^3v\, \boldsymbol{v}_\mathrm{D}^\alpha K_\alpha f_1^\alpha$ is the total energy flux, and $n_\alpha \boldsymbol{u} \cdot \boldsymbol{B} = B \int \mathrm{d}^3v\, v_\parallel f_1^\alpha$. Note that the least entropy production rate σ_*^α is described as $\sigma_*^\alpha = -\dot{S}_*^\alpha > 0$, which is positive definite.

2.2. Behavior of the velocity dependent diffusion coefficient

By using the variational method for Eq. (6) (see Ref. [2]), the energy integrated transport coefficients L_{jk}^α at a given magnetic flux surface labeled by $\rho =$ constant are given as

$$L_{jk}^\alpha = \frac{v_\mathrm{th}^\alpha}{\sqrt{\pi}} \left(\frac{B v_\mathrm{th}^\alpha}{\Omega_\alpha} \right)^2 \int_0^\infty \mathrm{d}K_\alpha\ K_\alpha{}^{j+k} \exp\{-K_\alpha\}\, D_{11}(K_\alpha), \tag{11}$$

where $1 \le j, k \le 2$. Here, the particle diffusivity and the thermal diffusivity are represented by L_{11}^α and L_{22}^α, respectively. Values $D_{11}(K_\alpha)$ are the *velocity dependent diffusion coefficients* calculated by using the DKES code [2]. The diffusion coefficients D_{11} are given as a function of the inverse of the mean free path $\mathsf{CMUL} \equiv \nu/v$ and the radial

electric field parameter EFIELD $\equiv E_\rho/v$ (see Figs. 1 and 2). The velocity dependent diffusion coefficients D_{11} are interpreted as mono-energetic diffusion coefficients. Hereafter we use the effective minor radius r to designate the label of the magnetic flux surface ρ, where the effective minor radius r is defined by $r/a = \sqrt{\Phi_{\rm normal}}$ and a is the plasma minor radius.

Let us compare the diffusion coefficients D_{11} obtained from the DKES code to analytical results of Refs. [10] and [11]. As shown below, we can represent mono-energetic diffusion coefficients under radial electric fields E_r and the simplified magnetic field model given as

$$B = B_0[1 - \epsilon_{\rm t}\cos\theta - \epsilon_{\rm h}\cos(L_{\rm p}\theta - M_{\rm p}\zeta)], \tag{12}$$

where $\epsilon_{\rm t}$ and $\epsilon_{\rm h}$ are the toroidal and helical ripples, and θ and ζ are the poloidal and toroidal angles, respectively. Here we assume $\epsilon_{\rm t} < \epsilon_{\rm h}$. From the viewpoint of mono-energetic particles, the diffusion coefficients D under radial electric fields are classified into [10]

$$D = \begin{cases} D_{1/\nu} & \propto & 1/\nu & \text{for } \epsilon_{\rm h}\omega_E < \nu \\ D_{\sqrt{\nu}} & \propto & \nu^{1/2}/{\omega_E}^{3/2} & \text{for } {\epsilon_{\rm t}}^2{\epsilon_{\rm h}}^{-1}\omega_E < \nu < \epsilon_{\rm h}\omega_E \\ D_{\nu} & \propto & \nu/{\omega_E}^2 & \text{for } \nu < {\epsilon_{\rm t}}^2{\epsilon_{\rm h}}^{-1}\omega_E, \end{cases} \tag{13}$$

where $\omega_E = E_r/rB$ and $E_r = (\mathrm{d}\rho/\mathrm{d}r)\,E_\rho$.

The magnetic field strength of the LHD is represented as

$$B = \sum_{\ell,m} B_{\ell m}\cos(\ell\theta - m\zeta), \tag{14}$$

where ℓ ($\ell = 0, 1, 2, 3, \cdots$) and $m = pM_{\rm p}$ ($p = 0, \pm1, \pm2, \pm3, \cdots$) are the poloidal and toroidal mode numbers, respectively. Main terms (*i.e.* the largest three components) of B of the standard configuration $\Delta_{\rm v} = -0.15$ [m] with $\beta_0 = 0\%$ are B_{00}, $B_{10}\cos\theta$, and $B_{2\ 10}\cos(2\theta - 10\zeta)$ (see Fig. 3(a)). The ripples are given as $\epsilon_{\rm t} = B_{10}/B_{00}$ and $\epsilon_{\rm h} = B_{2\ 10}/B_{00}$, respectively. Therefore, the magnetic field strength can be approximately represented as Eq. (12), and the ripples are estimated $\epsilon_{\rm t} = 0.11$ and $\epsilon_{\rm h} = 0.14$ at $(r/a) = 0.8$. Next, we compare D_{11} in Fig. 1(a) with Eq. (13) in this case. As shown

in Fig. 1(a), we have three slopes on a line with a fixed EFIELD, *i.e.* there are the ν, $\nu^{1/2}$, and $1/\nu$ regimes. In the ν and $\nu^{1/2}$ regimes, D_{11} has dependence on the electric fields E_r and decreases when EFIELD increases. On the other hand, in the $1/\nu$ regime it is independent of E_r. For a fixed nonzero EFIELD, if CMUL is decreasing, the slope of D_{11} changes from $1/\nu$ to $\nu^{1/2}$ and finally to ν. In our calculation, the critical value of CMUL from $1/\nu$ to $\nu^{1/2}$ is estimated as $\sim \epsilon_h$EFIELD and agrees with Eq. (13). From Fig. 1(a), we can show easily that values of D_{11} in the $\nu^{1/2}$ regime are proportional to CMUL$^{1/2}$/EFIELD$^{3/2}$, as given by heuristic-derived results Eq. (13). The critical value of CMUL from $\nu^{1/2}$ to ν, however, is different from the scaling $\sim \epsilon_t{}^2\epsilon_h{}^{-1}$EFIELD.

Next, let us examine the case of $\epsilon_t > \epsilon_h$ in the standard configuration $\Delta_v = -0.15$ [m] with $\beta_0 = 0\%$. The behavior of D_{11} for $\epsilon_t = 0.07$ and $\epsilon_h = 0.05$ at $(r/a) = 0.5$ is shown in Fig. 1(b). In this case, the diffusion coefficients D_{11} are also classified into the ν, $\nu^{1/2}$, and $1/\nu$ regimes. From Fig. 1(b), the critical value of CMUL from $1/\nu$ to $\nu^{1/2}$ is obtained by $\sim \epsilon_h$EFIELD, even if $\epsilon_t > \epsilon_h$. This result can be explained by effects of the helical ripple ϵ_h, and effects of the toroidal ripple ϵ_t may be negligible at this critical point. This result is interpreted by the estimation of Ref. [10]. When there is no radial electric field, orbits contributing to the transport deviate significantly from magnetic flux surfaces by the ∇B drift in the right hand side of Eq. (3), thus the diffusion coefficients are proportional to $1/\nu$ in the regime satisfying $\nu/\epsilon_h > \omega_h$, where $\omega_h = \epsilon_h T/(er^2B)$. While, under the radial electric fields with $\omega_E/\omega_h > 1$ the $\boldsymbol{E} \times \boldsymbol{B}$ drift in the left hand side of Eq. (3) cancels the ∇B drift and the orbits are close to the flux surfaces (*i.e.* the transport is improved significantly), thus the $1/\nu$ regime is suppressed into the regime $\omega_E > \nu/\epsilon_h > \omega_h$ and the $\nu^{1/2}$ regime may appear in $\nu/\epsilon_h < \omega_E$.

Now, we examine effects of finite-β on the diffusion coefficients D_{11}, comparing Fig. 2 with Fig. 1. In general, the difference between orbits of deeply trapped particles and magnetic flux surfaces becomes large as the β value increases [12, 13], thus we can expect easily that the transport coefficients of $\beta_0 = 6\%$ is larger than those of 0%. By making a comparison between cases of $\beta_0 = 0\%$ and 6%, we can see effects of a deformation

of magnetic flux surfaces on the diffusion coefficients D_{11}. For the same value of the radial electric fields, D_{11} becomes larger with an increase in the β value. From the calculations in Fig. 1(b) and Fig. 2(b), it is found that D_{11} with $\beta_0 = 6\%$ is about two times larger than that with $\beta_0 = 0\%$. This result is caused from the effect of helical ripples $B_{\ell m}$ with $(\ell, m) = (2+p, 10)$; $p = -2, -1, 1, 2, \cdots$, (see Refs. [6, 14]), which are the same order of magnitude as the component $(\ell, m) = (2, 10)$. Actually, we notices a deformation of the structure of the magnetic field by finite-β as follows. In Fig. 3, the main components $(\ell, m) = (0, 0)$, $(1, 0)$, $(2, 10)$ are dominant over all of the Fourier components of the vacuum magnetic field strength, while in the finite-β ($\beta_0 = 6\%$) magnetic field, amplitudes of the Fourier components with $(2+p, 10)$ are the same order as of the main components and helical ripples are located to the outside of the torus.

Hereafter, by using Eq. (11), we calculate the transport coefficients at $r/a = 0.5$ for the several configurations. In general, the transport coefficients at $r/a = 0.8$ are smaller than at $r/a = 0.5$ because of a lower temperature at $r/a = 0.8$.

3. Transport coefficients and radial electric fields determined under the ambipolarity condition

By performing the integration of Eq. (11), we can obtain the transport coefficients. Particle diffusivities of ions L_{11}^{i} and electrons L_{11}^{e} are shown in Fig. 4. When the temperature of the plasma is about one keV (we assume $T_{\mathrm{i}} = T_{\mathrm{e}} = T$ and $n_{\mathrm{i}} = n_{\mathrm{e}} = (\beta_0 B_0 / 4\mu_0 T)\left[1 - (r/a)^2\right]^2$, where $mu_0 = 4\pi \times 10^{-7}$ [henry/m]), both of ions and electrons are in the $1/\nu$ regime. While, if the plasma under large electrostatic potential differences $|e\phi/T| \geq 1$ has the temperature of several keV, for example, $T = 4.64$ [keV] (*i.e.* $1/T^{3/2} = 10^{-1}$), ions are in the $\nu^{1/2}$ regime and electrons are in the $1/\nu$ regime, where ϕ is the electrostatic potential, $-\mathrm{d}\phi/\mathrm{d}r = \phi/a = E_r$, and is defined as $\phi(r = a) \equiv 0$.

The diffusion of plasma across a magnetic flux surface is determined by the ambipo-

larity condition:

$$J_r \equiv e\Gamma_r^{\mathrm{i}} - e\Gamma_r^{\mathrm{e}} = 0, \tag{15}$$

where $J_r = e(\boldsymbol{\Gamma}_{\mathrm{i}} - \boldsymbol{\Gamma}_{\mathrm{e}}) \cdot \nabla r$ is the radial net current across a magnetic flux surface, $\Gamma_r^{\mathrm{i}} = \boldsymbol{\Gamma}_{\mathrm{i}} \cdot \nabla r = -n_{\mathrm{i}}(L_{11}^{\mathrm{i}} A_1^{\mathrm{i}} + L_{12}^{\mathrm{i}} A_2^{\mathrm{i}})$, and $\Gamma_r^{\mathrm{e}} = \boldsymbol{\Gamma}_{\mathrm{e}} \cdot \nabla r = -n_{\mathrm{e}}(L_{11}^{\mathrm{e}} A_1^{\mathrm{e}} + L_{12}^{\mathrm{e}} A_2^{\mathrm{e}})$. Here, A_1^α and A_2^α are rewritten as

$$A_1^\alpha = \frac{\mathrm{d}\ln n_\alpha}{\mathrm{d}r} - \frac{3}{2}\frac{\mathrm{d}\ln T_\alpha}{\mathrm{d}r} + \left(\frac{e_\alpha \phi}{T_\alpha}\right)\frac{\mathrm{d}\ln \phi}{\mathrm{d}r}, \tag{16a}$$

$$A_2^\alpha = \frac{\mathrm{d}\ln T_\alpha}{\mathrm{d}r}. \tag{16b}$$

Note that we assume $\left\langle E_{\parallel} \right\rangle = \langle \boldsymbol{E} \cdot \boldsymbol{b} \rangle = 0$, *i.e.* $A_3^\alpha = 0$. Both the transport coefficients L_{jk}^α and the forces A_1^α depend on the radial electric fields $E_r = -\mathrm{d}\phi/\mathrm{d}r$, thus Eq. (15) is a nonlinear equation for E_r, and by solving this equation at a fixed temperature, the radial electric field is determined.

Before calculating radial electric fields and the transport coefficients under the ambipolarity condition, we try to understand qualitatively the behavior of the particle fluxes under $|e\phi/T_\alpha| \approx 1$. The transport coefficients L_{jk}^α are independent of the sign of the radial electric fields E_r because of the stellarator symmetry of the magnetic field (see Ref. [15]). We assume that ions and electrons contributing to the transport are in the $\nu^{1/2}$ regime and in the $1/\nu$ regime, respectively. Since the transport coefficients in the $\nu^{1/2}$ regime are even functions of E_r and generally decrease with E_r increases, the coefficients of ions may be written as

$$L_{jk}^{\mathrm{i}} = \frac{L_{jk}^{\mathrm{i}(0)}}{1 + l_{jk}^{\mathrm{i}} E_r^{\,2}}, \tag{17}$$

where $L_{jk}^{\alpha(0)}$ and l_{jk}^α are independent of E_r. On the other hand, in the $1/\nu$ regime the transport coefficients are independent of E_r, so that the coefficients of electrons are

$$L_{jk}^{\mathrm{e}} = L_{jk}^{\mathrm{e}(0)}. \tag{18}$$

Thus, we can represent the particle fluxes of ions and electrons as follows.

$$\Gamma_r^{\mathrm{i}} = -\sum_{k=1}^{2} n_{\mathrm{i}} L_{1k}^{\mathrm{i}} A_k^{\mathrm{i}}$$

$$= -n_{\rm i}\left\{\frac{L_{11}^{\rm i(0)}}{1+l_{11}^{\rm i}{E_r}^2}\left(\frac{{\rm d}\ln n_{\rm i}}{{\rm d}r}-\frac{3}{2}\frac{{\rm d}\ln T_{\rm i}}{{\rm d}r}-\frac{eE_r}{T_{\rm i}}\right)\right.$$
$$\left.+\frac{L_{12}^{\rm i(0)}}{1+l_{12}^{\rm i}{E_r}^2}\left(\frac{{\rm d}\ln T_{\rm i}}{{\rm d}r}\right)\right\}, \tag{19a}$$

$$\Gamma_r^{\rm e} = -\sum_{k=1}^{2} n_{\rm e}L_{1k}^{\rm e}A_k^{\rm e}$$
$$= -n_{\rm e}\left\{L_{11}^{\rm e(0)}\left(\frac{{\rm d}\ln n_{\rm e}}{{\rm d}r}-\frac{3}{2}\frac{{\rm d}\ln T_{\rm e}}{{\rm d}r}+\frac{eE_r}{T_{\rm e}}\right)\right.$$
$$\left.+L_{12}^{\rm e(0)}\left(\frac{{\rm d}\ln T_{\rm e}}{{\rm d}r}\right)\right\}. \tag{19b}$$

Therefore a bifurcation of solutions to Eq. (15) can appear. If both of ions and electrons are in the $1/\nu$ regime, the particle fluxes can be represented as

$$\Gamma_r^{\alpha} = -n_{\alpha}\left\{L_{11}^{\alpha(0)}\left(\frac{{\rm d}\ln n_{\alpha}}{{\rm d}r}-\frac{3}{2}\frac{{\rm d}\ln T_{\alpha}}{{\rm d}r}-\frac{e_{\alpha}E_r}{T_{\alpha}}\right)\right.$$
$$\left.+L_{12}^{\alpha(0)}\left(\frac{{\rm d}\ln T_{\alpha}}{{\rm d}r}\right)\right\}. \tag{20}$$

In this case, both of $\Gamma_r^{\rm i}$ and $\Gamma_r^{\rm e}$ are linear functions of electric fields E_r, so that a number of solutions of Eq. (15) is only one.

To actually calculate the particle fluxes, we assume the following relations:

$$\frac{{\rm d}\ln n_{\alpha}}{{\rm d}r}=\frac{{\rm d}\ln T_{\alpha}}{{\rm d}r}=-\frac{E_r}{\phi}, \tag{21}$$

$n_{\rm i}=n_{\rm e}=n$, and $T_{\rm i}=T_{\rm e}=T$, where $-E_r/\phi={\rm d}\ln\phi/{\rm d}r$. Under this assumption, the total flux $\Gamma_r^{\rm total}$ for a fixed temperature T can be calculated as in Fig. 5. In Figs. 5(a) and (c), the temperature of the plasma is 1 [keV]. Both ions and electrons are in the $1/\nu$ regime, so that we can understand easily the behavior of $\Gamma_r^{\rm total}$ by using Eq. (20). While, in Figs. 5(b) and (d), the temperature is 4.64 [keV]. For the vacuum case, ions are in the $\nu^{1/2}$ regime and electrons are in the $1/\nu$ regime (see Figs. 4(a) and (b)). On the other hand, for the finite-β case, ions are in the $\nu^{1/2}$ regime and electrons are in the transient regime between the $1/\nu$ and $\nu^{1/2}$ regimes (see Figs. 4(c) and (d)). In the vacuum case, the behavior of $\Gamma_r^{\rm total}$ can be explained by using Eqs. (19a) and (19b). However, in the finite-β ($\beta_0=6\%$) case, a behavior of $\Gamma_r^{\rm e}$ is different from Eq. (19b), because the

transport coefficients depend on electric fields as shown in Fig. 4(d). Electrons in the finite-β configuration are affected strongly by electric fields as compared with electrons in the vacuum.

Next, using Eq. (15), we determine the radial electric field E_r as in Table I, in particular, for the standard configuration $\Delta_v = -0.15$ [m] with $\beta_0 = 6\%$, E_r is calculated as in Fig. 6. In Fig. 6, we can see a bifurcation of E_r at $T = T_{c1} = 3.67$ [keV]. And there exist three roots of E_r satisfying Eq. (15) within a region $T_{c1} = 3.67$ [keV] $< T < T_{c2} = 5.54$ [keV] (*i.e.* $1.42 \times 10^{-1} > 1/T^{3/2} > 7.67 \times 10^{-2}$). If the temperature T is greater than T_{c1}, then the large positive electric fields which correspond to the electron roots can be realized. When the temperature T increases from some low temperature ($T < T_{c1}$). however, we may not observe the electron root, because the plasma chooses the electric fields E_r given by the line of the ion root until $T = T_{c2}$. Therefore, to induce the electron root in the plasma with $T < T_{c2}$, we may need to heat electrons.

After determining radial electric fields E_r, we can calculate the transport coefficients. In particular, we are interested in the thermal diffusivity for the only thermal conduction. Note that the thermodynamic flux I_2^α defined in the DKES code denotes the total energy flux, (see Eq. (10b)). To calculate the thermal diffusivity, we need to separate the total energy flux $\boldsymbol{Q}_\alpha$ into the conduction part $\boldsymbol{q}_\alpha$ and the convection part $(5/2)T_\alpha \boldsymbol{\Gamma}_\alpha$, *i.e.* $\boldsymbol{Q}_\alpha = \boldsymbol{q}_\alpha + (5/2)T_\alpha \boldsymbol{\Gamma}_\alpha$, (see Ref. [16]). Now, we change definitions of pairs of fluxes and forces. New fluxes are

$$Y_1^\alpha = \langle \boldsymbol{\Gamma}_\alpha \cdot \nabla r \rangle, \tag{22a}$$

$$Y_2^\alpha = \left\langle \frac{\boldsymbol{q}_\alpha \cdot \nabla r}{T_\alpha} \right\rangle, \tag{22b}$$

and the conjugate forces are

$$X_1^\alpha = \frac{\mathrm{d} \ln n_\alpha}{\mathrm{d}r} + \frac{\mathrm{d} \ln T_\alpha}{\mathrm{d}r} + \left(\frac{e_\alpha \phi}{T_\alpha} \right) \frac{\mathrm{d} \ln \phi}{\mathrm{d}r}, \tag{23a}$$

$$X_2^\alpha = \frac{\mathrm{d} \ln T_\alpha}{\mathrm{d}r}. \tag{23b}$$

In this case, the fluxes are described by using the forces as

$$\begin{pmatrix} Y_1^\alpha \\ Y_2^\alpha \end{pmatrix} = -n_\alpha \mathsf{N}_\alpha \begin{pmatrix} X_1^\alpha \\ X_2^\alpha \end{pmatrix}, \tag{24}$$

where N_α is defined by

$$\mathsf{N}_\alpha \equiv \begin{pmatrix} N_{11}^\alpha & N_{12}^\alpha \\ N_{21}^\alpha & N_{22}^\alpha \end{pmatrix}, \tag{25}$$

and N_{jk}^α are new transport coefficients. The relation between A_j^α and X_j^α is

$$\begin{pmatrix} A_1^\alpha \\ A_2^\alpha \end{pmatrix} = \mathsf{T} \begin{pmatrix} X_1^\alpha \\ X_2^\alpha \end{pmatrix}, \tag{26}$$

where the tensor T is defined by

$$\mathsf{T} \equiv \begin{pmatrix} 1 & -5/2 \\ 0 & 1 \end{pmatrix}. \tag{27}$$

Even if pairs of fluxes and forces are changed, the least entropy production rate σ_*^α does not change [17]:

$$\sigma_*^\alpha = -\sum_{j=1}^{2} I_j^\alpha A_j^\alpha = -\sum_{k=1}^{2} Y_k^\alpha X_k^\alpha. \tag{28}$$

Thus N_{jk}^α are described by L_{jk}^α as

$$\mathsf{N}_\alpha = \mathsf{T}^{\mathrm{t}}\, \mathsf{L}_\alpha\, \mathsf{T}, \tag{29}$$

where T^{t} is the transpose of T and $\mathsf{L}_\alpha \equiv \left(L_{jk}^\alpha\right)$. Then we can calculate the thermal diffusivity N_{22}^α for the thermal conduction, using Eqs. (15) and (29). Note that $N_{11}^\alpha = L_{11}^\alpha$. We obtain the particle diffusivities N_{11}^α and the thermal diffusivities N_{22}^α as in Table I. In particular, for the standard configuration $\Delta_{\mathrm{v}} = -0.15$ [m] with $\beta_0 = 6\%$, N_{11}^α and N_{22}^α are calculated as in Fig. 7. In these figures, we can see that if the temperature is greater than $T_{\mathrm{c1}} = 3.67$ [keV], the transport coefficients are improved significantly by large positive electric fields which correspond to the electron roots.

If the electron root is realized, then the large positive radial electric field appears, thus the transport coefficients for ions with $T_{\mathrm{i}} = T_{\mathrm{e}} = T = 4.64$ [keV] can be suppressed

within the same order of the coefficients for the one keV plasma (see Table I). Although the $\boldsymbol{E} \times \boldsymbol{B}$ drift can suppress the transport coefficients for ions as shown in Table I, the coefficients of electrons are insensitive to the electric field, because the thermal velocity of electrons is much faster than the $\boldsymbol{E} \times \boldsymbol{B}$ drift velocity.

On the other hand, in the inward-shifted configuration $\Delta_{\rm v} = -0.25$ [m] with $\beta_0 = 0, 8\%$ the transport coefficients are improved as shown in Tables I(c) and (d), because the helical ripples are localized to the inside of the torus as shown in Fig. 3(c) and orbits contributing dominantly to the transport are improved [6, 5]. By transferring the vacuum magnetic axis inward, the the helical ripples move to the inside of the torus (see Figs. 3(a) and (c)).

From Table I, it is found that the transport coefficients increase with the temperature increases. When the temperature changes from $T = 1$ [keV] to 4.64 [keV] in the standard configuration $\Delta_{\rm v} = -0.15$ [m] with $\beta_0 = 6\%$, the coefficients for ions and electrons change one order and two order larger, respectively, if the plasma stays on the ion root. Especially, the electron thermal diffusivity $N^{\rm e}_{22}$ is too large; $N^{\rm e}_{22} \approx 73$ [m^2/sec] in the standard configuration. A characteristic time of thermal conduction of electrons is estimated as $\tau^{\rm e}_T = a^2/N^{\rm e}_{22}$, where a is the plasma radius. In this case, we have $\tau^{\rm e}_T \approx 4.90 \times 10^{-3}$ [sec] and the ion-electron collision time $\tau_{\rm ie} \approx 5.84 \times 10^{-2}$ [sec]. Thus the electron thermal conduction proceeds faster than the isothermalization between ions and electrons, so that the temperature of electrons can become lower than of ions in the transport time scale. Then we assume $T_{\rm i} \approx 2T_{\rm e}$, and re-calculate the transport coefficients under the ambipolarity condition, as shown in Table II. If this situation is realized, all of the transport coefficients for the high temperature plasma ($T_{\rm i} = 4.64$ [keV] and $T_{\rm e} = 2.15$ [keV]) are suppressed within about 2 [m^2/sec], and the energy loss of electrons is limited to the acceptable value.

Finally, even if the ion temperature is low, to easily observe a bifurcation of radial electric fields, let us consider that only electrons are heated and the ion temperature $T_{\rm i}$ is fixed. Now, we set $T_{\rm i} = 1.5$ [keV]. If $T_{\rm e}/T_{\rm i} > 2.56$, then the bifurcation can appear,

(see Fig. 8).

4. SUMMARY

We have investigated effects of finite-β and radial electric fields on the neoclassical transport in the LHD configurations with $\Delta_v = -0.15$ [m], $\beta_0 = 0, 6\%$ and $\Delta_v = -0.25$ [m], $\beta_0 = 0, 8\%$. We have applied the DKES code to calculate the transport coefficients. We have found that the transport coefficients increase when the β value increases, but the coefficients for the finite-β case are improved significantly by radial electric fields determined by the ambipolarity condition.

In Fig. 4, the transport coefficients for $\beta_0 = 6\%$ are about two times larger than for $\beta_0 = 0\%$. This is caused mainly by the ripples with the Fourier components $(\ell, m) = (2 + p, 10)$, $p = -2, -1, 1, 2, \cdots$.

The radial electric fields have been determined under the ambipolarity condition. We have seen that the three roots of the electric fields are acceptable within some region of high temperature (*e.g.* see Fig. 6), there are two stable roots (ion and electron roots) and one unstable root. The obtained values of the electric fields and the transport coefficients have been shown in Table I. In the finite-β configurations, *i.e.* the standard configuration $\Delta_v = -0.15$ [m] with $\beta_0 = 6\%$ and the inward-shifted configuration $\Delta_v = -0.25$ [m] with $\beta_0 = 8\%$, if the plasma temperature is several keV, then the large positive electric fields are realized, and the transport coefficients of ions are reduced significantly. However, the coefficients of electrons keep large values as compared with those of ions. Especially the thermal diffusivity of electrons, N_{22}^{e}, is two order larger than of ions N_{22}^{i}. Based on the fact that N_{22}^{e} is too large as compared with N_{22}^{i}, we have assumed $T_i \approx 2T_e$ and re-calculated the transport coefficients (see Table II). From this calculation, we have found that the values of all of the transport coefficients of both ions and electrons are less than about 2 [m^2/sec].

Finally, we consider the situation that only electrons are heated and the ion temperature is fixed. If we set $T_i = 1.5$ [keV], then for $T_e/T_i > 2.56$ we may easily observe the

bifurcation of radial electric fields as compared with the situation of $T_i = T_e$.

ACKNOWLEDGEMENTS

One of the authors (R.K.) acknowledges fruitful discussions with Dr. J. Nuehrenberg and Dr. H. Maassberg about the transport in helical configurations. He also thanks Dr. K. Ichiguchi, Dr. S. Murakami, and Dr. C.D. Beidler for valuable discussions.

References

[1] IIYOSHI, A., FUJIWARA, M., MOTOJIMA, O., OYABU, N., YAMAZAKI, K., Fusion Technol. **17** (1990) 169.

[2] HIRSHMAN, S.P., SHAING, K.C., VAN RIJ, W.I., BEASLEY, C.O., Jr., CRUME, E.C., Jr., Phys. Fluids **29** (1986) 2951.

[3] VAN RIJ, W.I., HIRSHMAN, S.P., Phys. Fluids B **1** (1989) 563.

[4] RENNER, H., GASPARINO, U., MAASSBERG, H., et al., in Plasma Physics and Controlled Nuclear Fusion Research 1990 (Proc. 13th Int. Conf. Washington DC, 1990), Vol. 2, IAEA, Vienna (1991) 439.

[5] OGAWA, Y., AMANO, T., NAKAJIMA, N., YAMAZAKI, K., HIRSHMAN, S.P., VAN RIJ, W.I., SHAING, K.C., Nucl. Fusion **31** (1992) 119.

[6] MYNICK, H.E., CHU, T.K., BOOZER, A.H., Phys. Rev. Lett. **48** (1982) 322.

[7] HIRSHMAN, S.P., WHITSON, J.C., Phys. Fluids **26** (1983) 3553.

[8] HIRSHMAN, S.P., VAN RIJ, W.I., MERKEL, P., Comput. Phys. Commun. **43** (1986) 143.

[9] ICHIGUCHI, K., NAKAJIMA, N., OKAMOTO, M., NAKAMURA, Y., WAKATANI, M., Nucl. Fusion **33** (1993) 481.

[10] KADOMTSEV, B.B., POGUTSE, O.P., Nucl. Fusion **11** (1971) 67.

[11] MYNICK, H.E., Phys. Fluids **26** (1983) 2609.

[12] TODOROKI, J., J. Phys. Soc. Jpn. **59** (1990) 2758.

[13] NAKAMURA, Y., WAKATANI, M., LEBOEUF, J.-N., CARRERAS, B.A., DOMINGUEZ, N., HOLMES, J.A., LYNCH, V.E., PAINTER, S.L., GARCIA, L., Fusion Technol. **19** (1991) 217.

[14] SHAING, K.C., HOKIN, S.A., Phys. Fluids **26** (1983) 2136.

[15] HIRSHMAN, S.P., SHAING, K.C., VAN RIJ, W.I., Phys. Rev. Lett. **56** (1986) 1697.

[16] BALESCU, R., *Transport Processes in PLasmas* (North-Holland, Amsterdam, 1988) Vol.2, 668.

[17] DE GROOT, S.R., MAZUR, P., *Non-Equilibrium Thermodynamics* (Dover, New York, 1983) 77.

Figure captions

FIG. 1. Velocity dependent diffusion coefficients D_{11} *[1/mT^2] (calculated with the DKES code) as a function of the mean free path (denoted* CMUL $= \nu/v$ *[1/m]) at (a)* r/a *=0.8 and (b)* r/a *=0.5 in the standard configuration* $\Delta_v = -0.15$ *[m] with* β_0 *=0%. Here the radial electric fields are introduced by the parameter* EFIELD *(=* E_ρ/v *[V sec/m^2]).*

FIG. 2. Velocity dependent diffusion coefficients D_{11} *[1/mT^2] calculated at (a)* r/a *=0.8 and (b)* r/a *=0.5 in the standard configuration* $\Delta_v = -0.15$ *[m] with* β_0 *=6%.*

FIG. 3. Ripples $B_{\ell m}/B_{00}$ *for several Fourier mode numbers* (ℓ, m) *of the magnetic field strength as a function of the normalized effective minor radius* r/a *in the standard configurations* $\Delta_v = -0.15$ *[m] with (a)* β_0 *=0% and (b)* β_0 *=6%, and (c) in the inward-shifted configuration* $\Delta_v = -0.25$ *[m] with* β_0 *=0%. Here* B_{00} *is the amplitude of the (0,0) component of the magnetic field strength at the magnetic axis. In these figures, we show the largest seven components used in the calculations with the DKES code, except for* B_{00} *itself. The variation of the magnetic field strength B [T] along the magnetic field line is shown below as a function of the poloidal angle* θ *[degree]. Poloidal angles* 0 *and* 360 *degrees correspond to the outside of the torus, and* 180 *degrees is the inside of the torus.*

FIG. 4. Particle diffusivities L^α_{11} *[m^2/sec] as a function of a temperature in the standard configuration* $\Delta_v = -0.15$ *[m] with* β_0 *=0% for (a) ions* $\alpha = \mathrm{i}$ *and (b) electrons* $\alpha = \mathrm{e}$*, and with* β_0 *=6% for (c) ions and (d) electrons. Here the normalized electrostatic potential* $e\phi/T$ *is used instead of the radial electric fields* E_r*, where* $T_\mathrm{i} = T_\mathrm{e} = T$*. Values* $1/T^{3/2}$ *=0.03, 0.1, 1 correspond to T =10, 4.64, 1 [keV], respectively. From the stellarator symmetry of the magnetic field,* L^α_{11} *are independent of the sign of* $e\phi/T$*, see Ref.[15].*

FIG. 5. Particle fluxes Γ_r *[10^{23}/m^{2}sec] as a function of the normalized electrostatic*

potential $e\phi/T$ in the standard configurations $\Delta_v = -0.15$ [m] with (a) β_0 =0% and T =1 [keV], (b) β_0 =0% and T =4.64 [keV], (c) β_0 =6% and T =1 [keV], (d) β_0 =6% and T =4.64 [keV]. Here $T_i = T_e = T$.

FIG. 6. Radial electric fields E_r [kV/m] (defined by the ambipolarity condition) as a function of the temperature $T(= T_i = T_e)$ [keV] in the standard configuration $\Delta_v = -0.15$ [m] with β_0 =6%. Here $1/T^{3/2}$ =0.03, 0.1, 1 correspond to T =10, 4.64, 1 [keV], respectively.

FIG. 7. Particle diffusivities N^{α}_{11} [m^2/sec] of (a) ions $\alpha = i$ and (b) electrons $\alpha = e$, and thermal diffusivities N^{α}_{22} [m^2/sec] of (c) ions and (d) electrons. These are given as a function of the temperature $T(= T_i = T_e)$ [keV] in the standard configuration $\Delta_v = -0.15$ [m] with β_0 =6%. Here $1/T^{3/2}$ =0.03, 0.1, 1 correspond to T =10, 4.64, 1 [keV], respectively.

FIG. 8. Radial electric fields E_r [kV/m] (defined by the ambipolarity condition) as a function of the rate of electron and ion temperatures, T_e/T_i, in the standard configuration $\Delta_v = -0.15$ [m] with $\beta_0 = 6\%$. Here, the ion temperature is fixed at $T_i = 1.5$ [keV]. At $T_e/T_i \approx 2.56$, we can see the bifurcation of E_r.

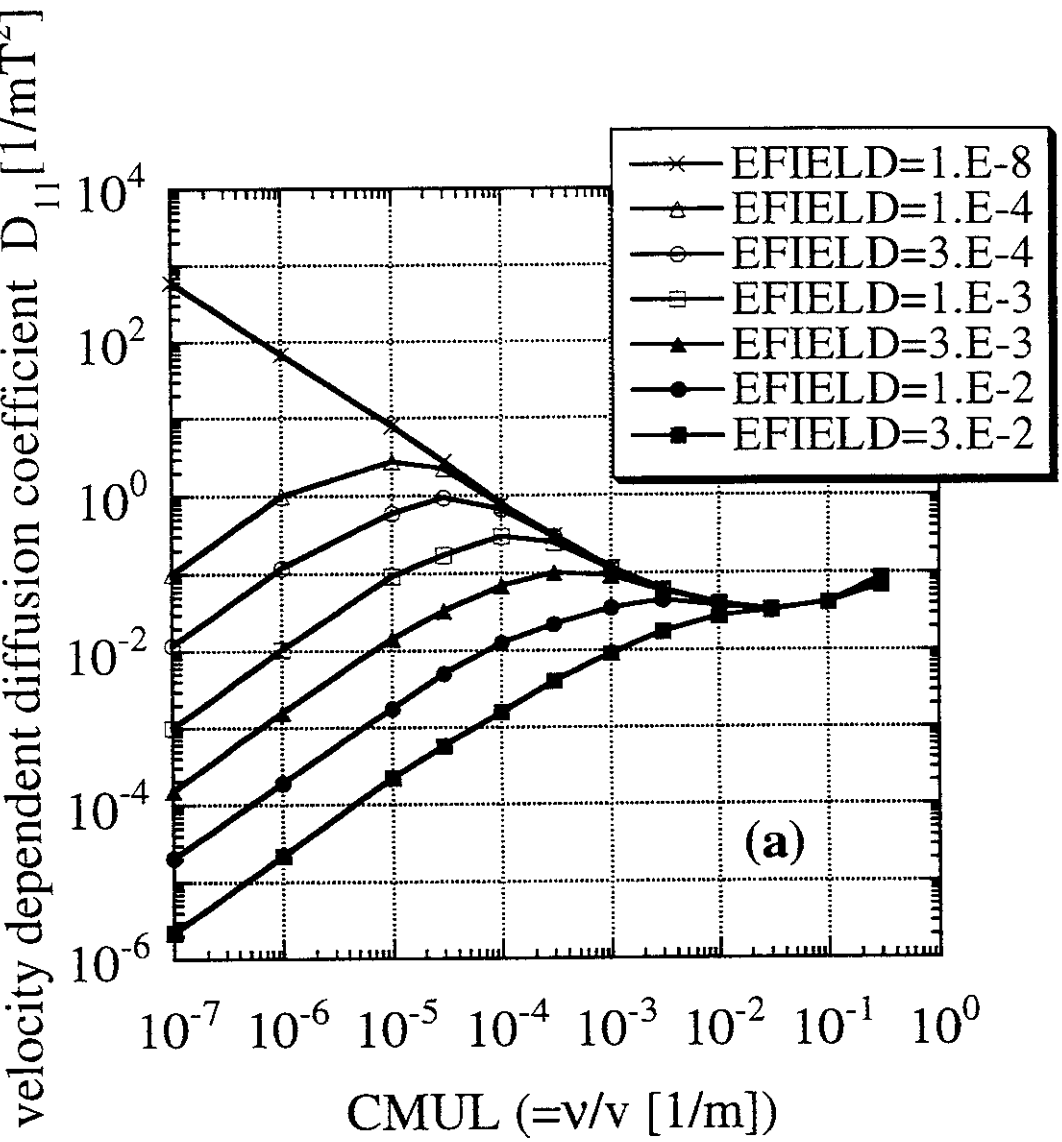
velocity dependent diffusion coefficient D_{11} [1/mT^2]
10^4
10^2
10^0
10^{-2}
10^{-4}
10^{-6}
10^{-7} 10^{-6} 10^{-5} 10^{-4} 10^{-3} 10^{-2} 10^{-1} 10^0
CMUL (=ν/v [1/m])
EFIELD=1.E-8
EFIELD=1.E-4
EFIELD=3.E-4
EFIELD=1.E-3
EFIELD=3.E-3
EFIELD=1.E-2
EFIELD=3.E-2
(a)

Fig.1(a)

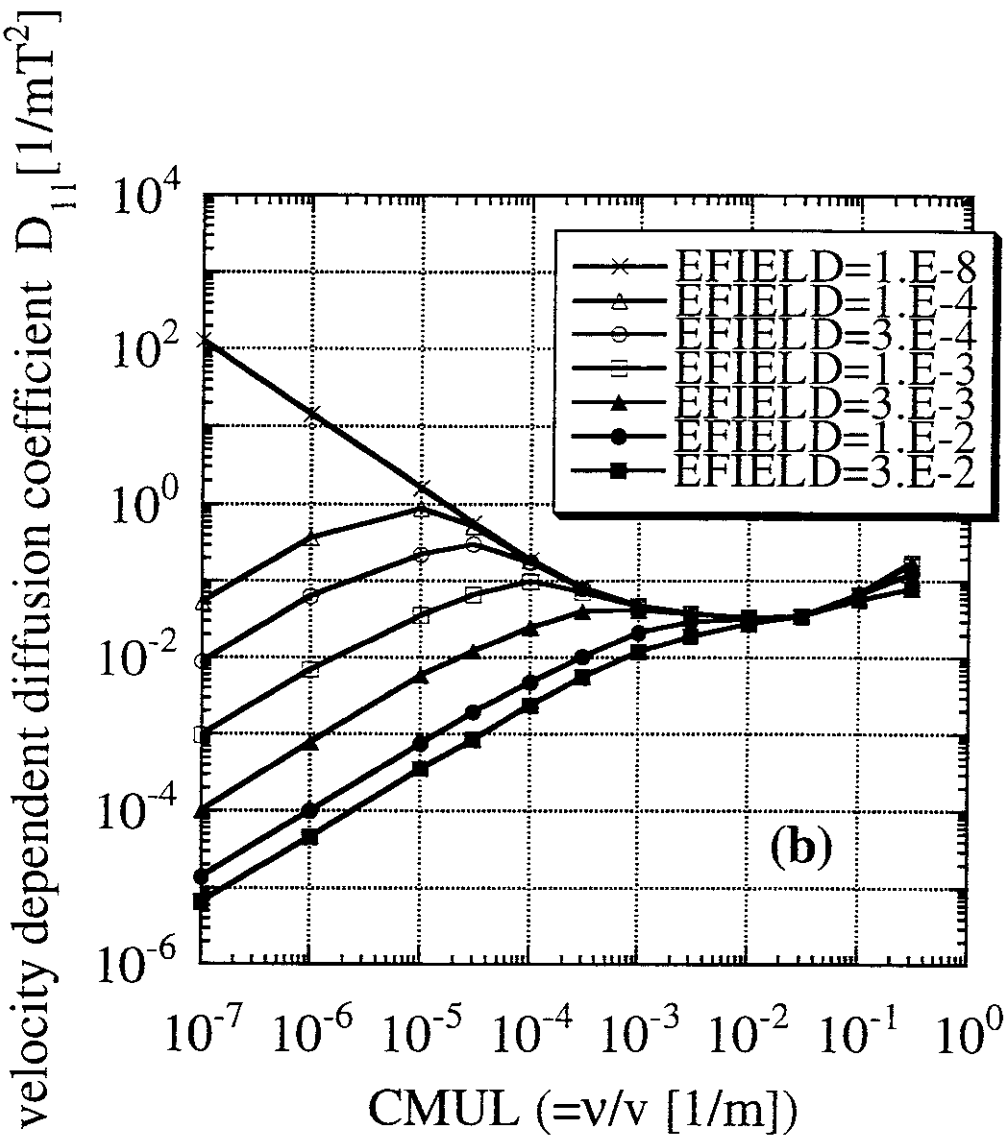
velocity dependent diffusion coefficient D_{11} [1/mT^2]
10^4
10^2
10^0
10^{-2}
10^{-4}
10^{-6}
EFIELD=1.E-8
EFIELD=1.E-4
EFIELD=3.E-4
EFIELD=1.E-3
EFIELD=3.E-3
EFIELD=1.E-2
EFIELD=3.E-2
(b)
10^{-7} 10^{-6} 10^{-5} 10^{-4} 10^{-3} 10^{-2} 10^{-1} 10^0
CMUL (=ν/v [1/m])

Fig.1(b)

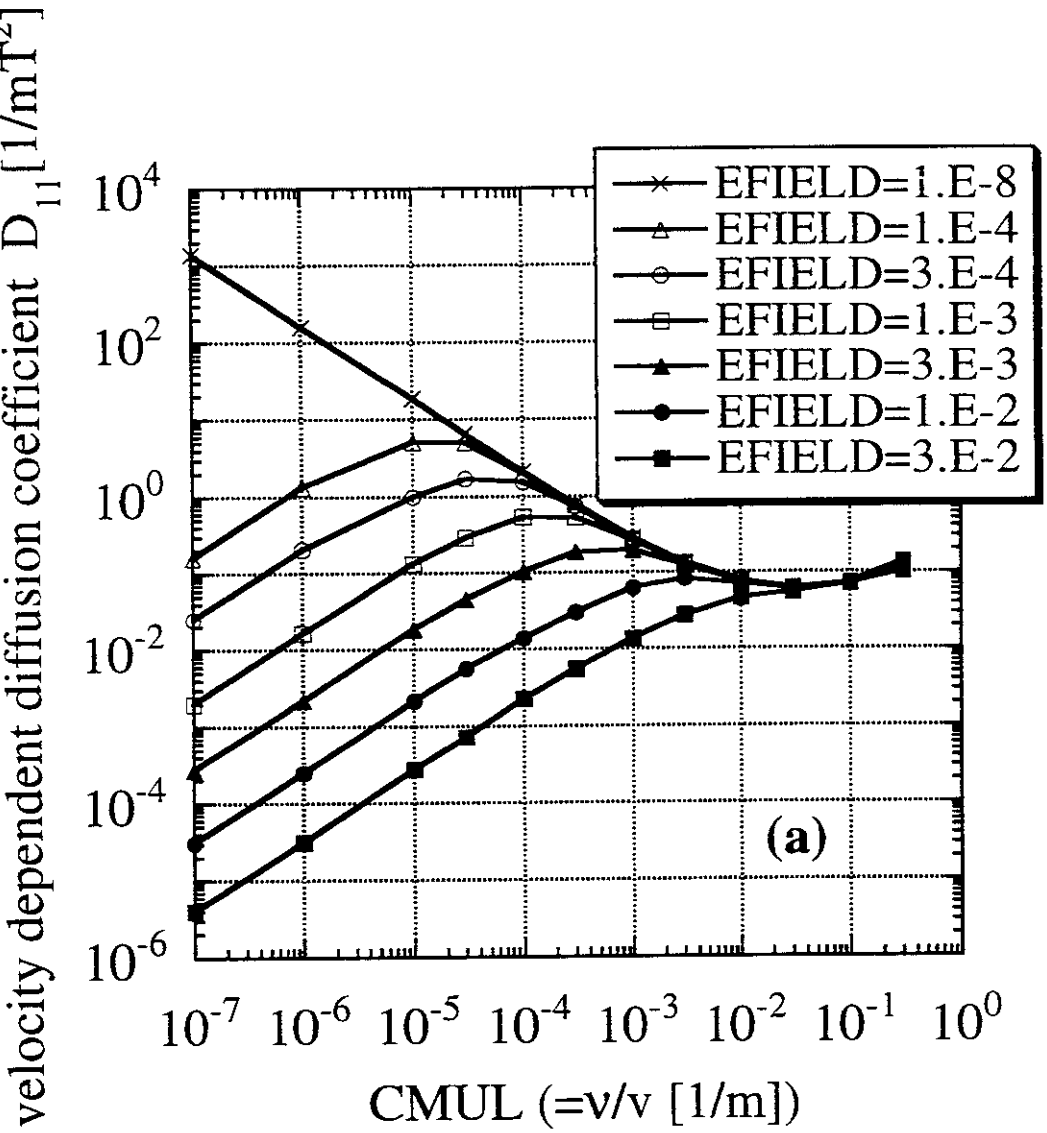
velocity dependent diffusion coefficient D_{11} [1/mT^2]
10^4
10^2
10^0
10^{-2}
10^{-4}
10^{-6}
EFIELD=1.E-8
EFIELD=1.E-4
EFIELD=3.E-4
EFIELD=1.E-3
EFIELD=3.E-3
EFIELD=1.E-2
EFIELD=3.E-2
(a)
10^{-7} 10^{-6} 10^{-5} 10^{-4} 10^{-3} 10^{-2} 10^{-1} 10^0
CMUL (=ν/v [1/m])

Fig.2(a)

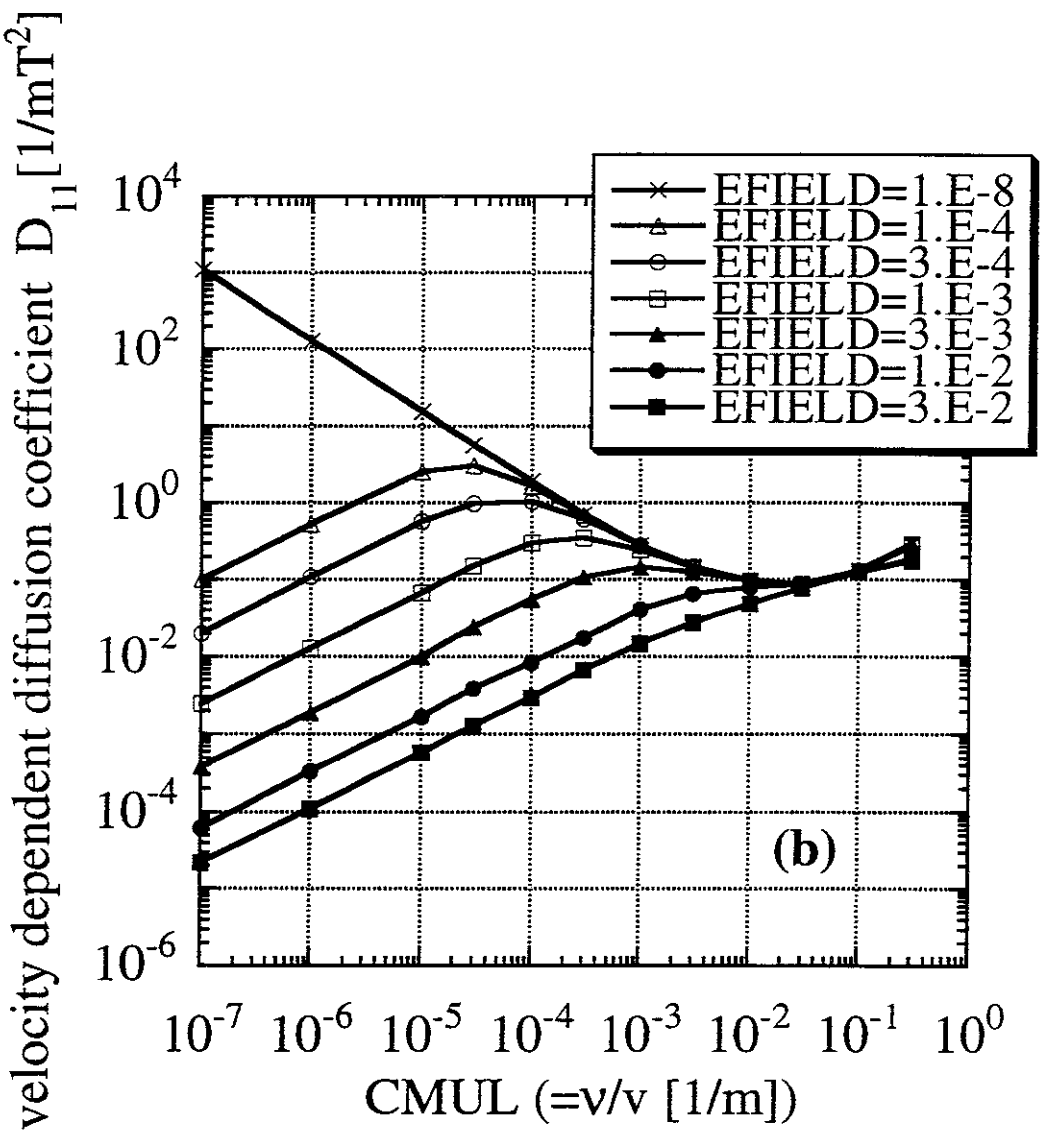
velocity dependent diffusion coefficient D_{11} [1/mT^2]
10^4
10^2
10^0
10^{-2}
10^{-4}
10^{-6}
EFIELD=1.E-8
EFIELD=1.E-4
EFIELD=3.E-4
EFIELD=1.E-3
EFIELD=3.E-3
EFIELD=1.E-2
EFIELD=3.E-2
(b)
10^{-7} 10^{-6} 10^{-5} 10^{-4} 10^{-3} 10^{-2} 10^{-1} 10^0
CMUL (=ν/v [1/m])

Fig.2(b)

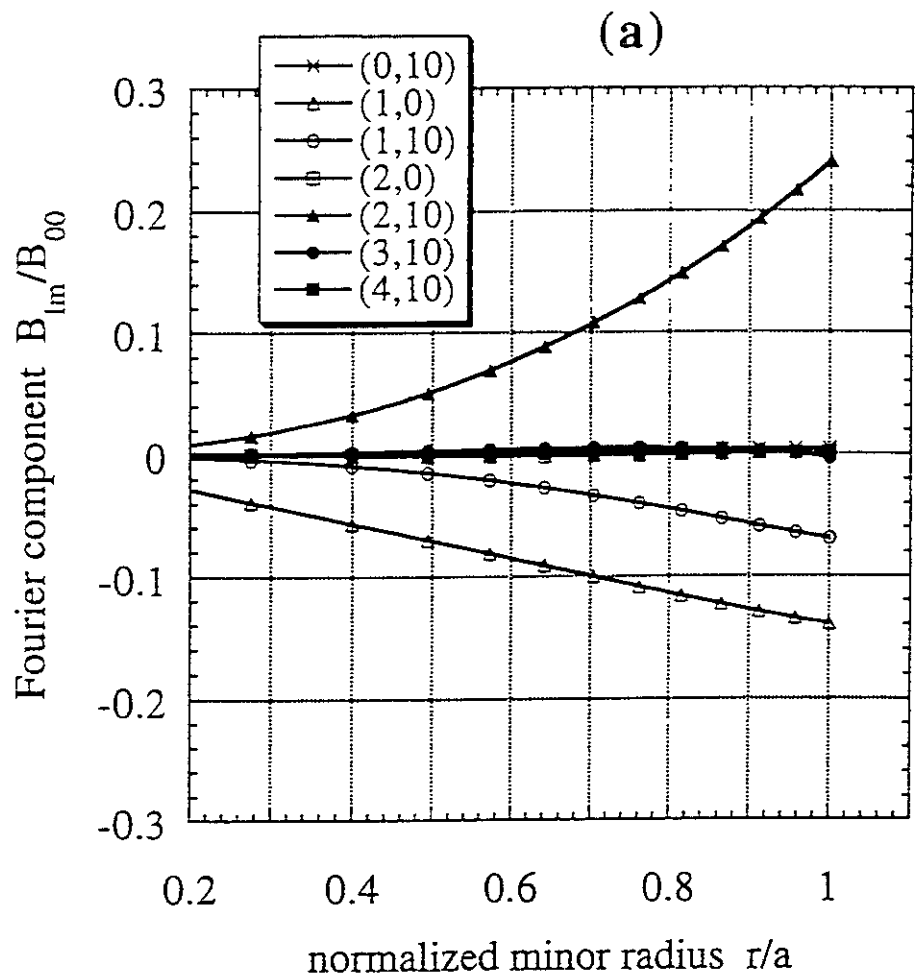
(a)
(0,10)
(1,0)
(1,10)
(2,0)
(2,10)
(3,10)
(4,10)
Fourier component B_{lm}/B_{00}
0.3
0.2
0.1
0
-0.1
-0.2
-0.3
0.2
0.4
0.6
0.8
1
normalized minor radius r/a

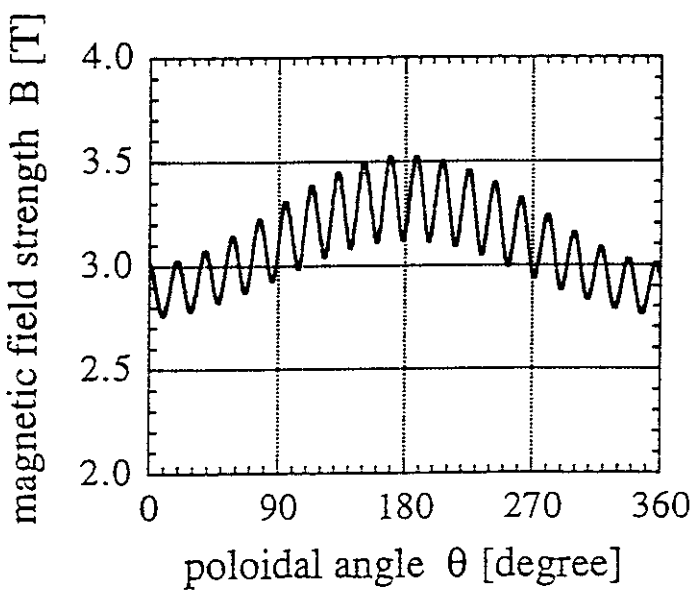
magnetic field strength B [T]
4.0
3.5
3.0
2.5
2.0
0
90
180
270
360
poloidal angle θ [degree]

Fig.3(a)

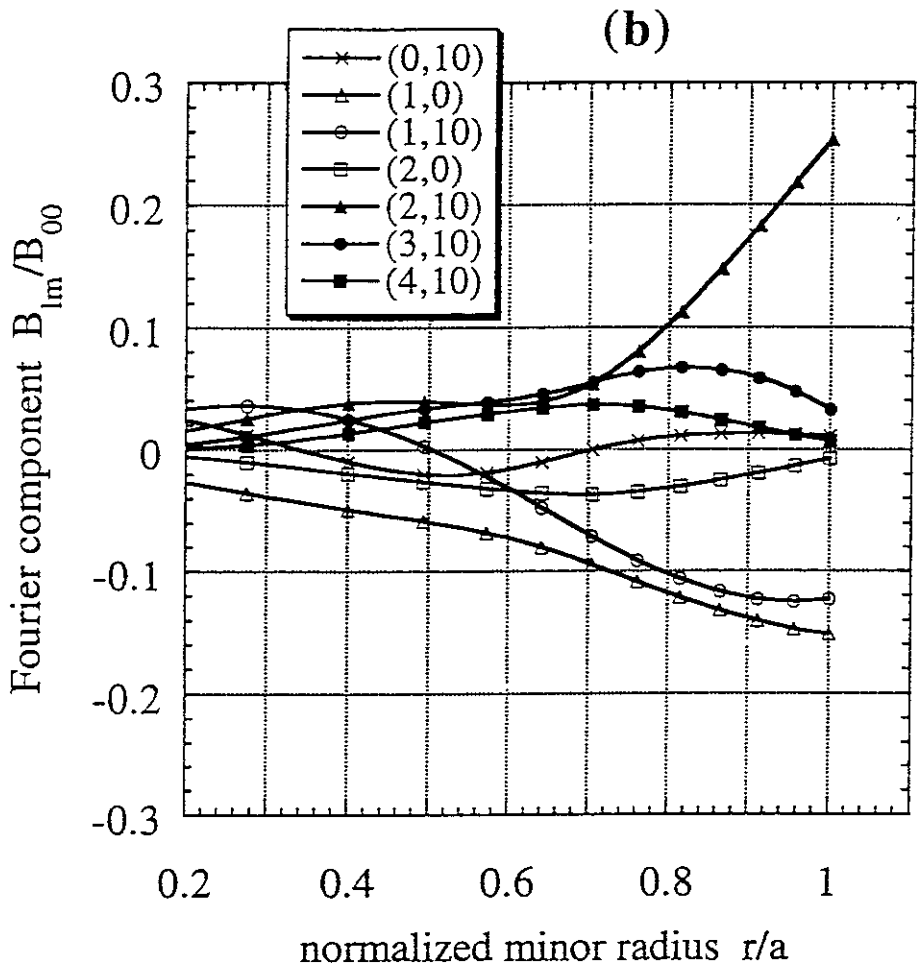
(b)
(0,10)
(1,0)
(1,10)
(2,0)
(2,10)
(3,10)
(4,10)
0.3
0.2
0.1
0
-0.1
-0.2
-0.3
Fourier component B_{lm}/B_{00}
0.2
0.4
0.6
0.8
1
normalized minor radius r/a

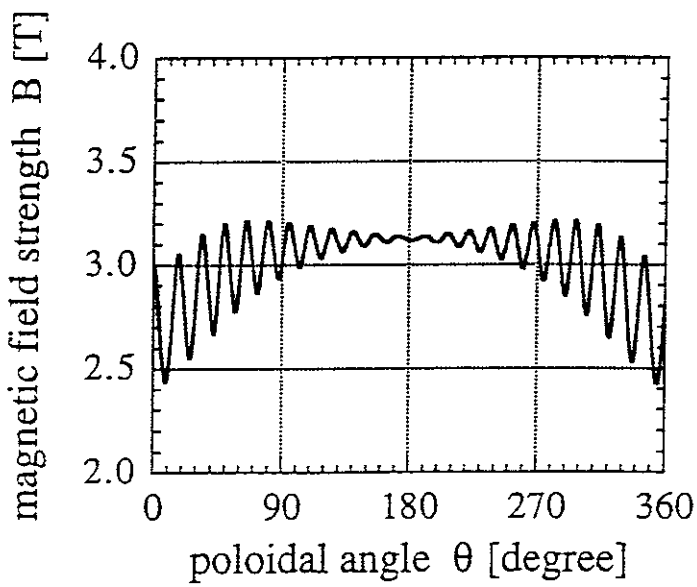
magnetic field strength B [T]
4.0
3.5
3.0
2.5
2.0
0
90
180
270
360
poloidal angle θ [degree]

Fig.3(b)

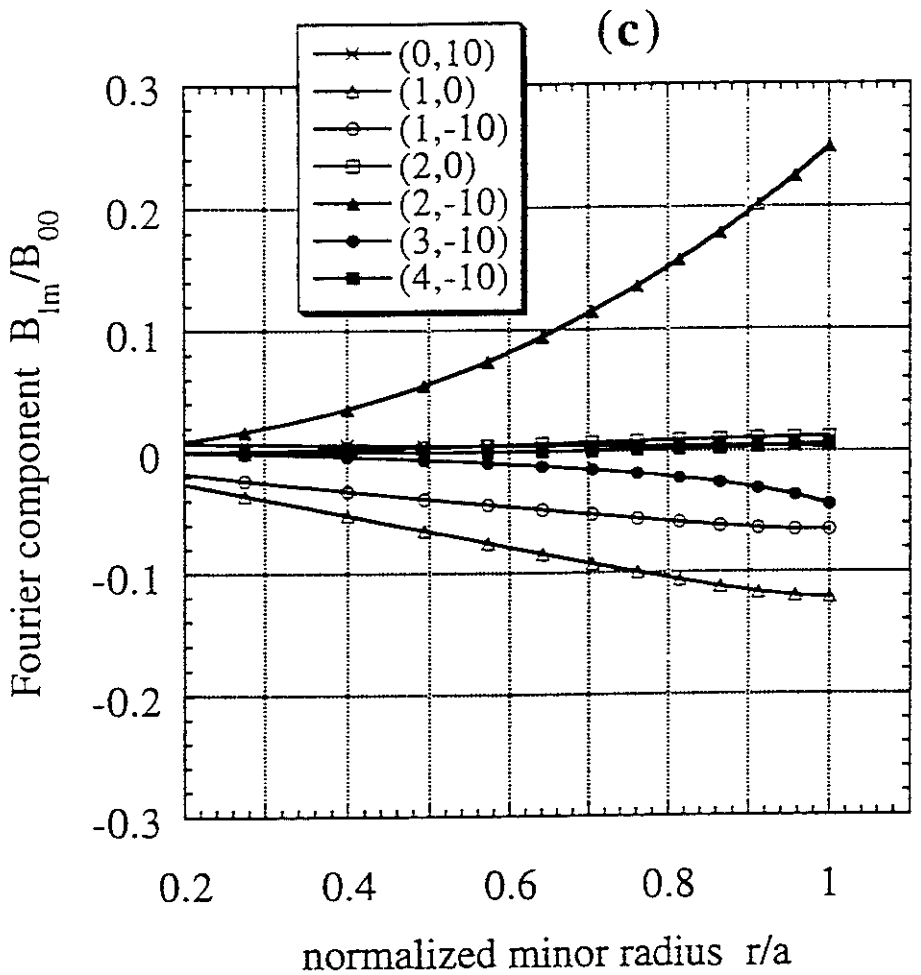
(c)
(0,10)
(1,0)
(1,-10)
(2,0)
(2,-10)
(3,-10)
(4,-10)
0.3
0.2
0.1
0
-0.1
-0.2
-0.3
Fourier component B_{lm}/B_{00}
0.2
0.4
0.6
0.8
1
normalized minor radius r/a

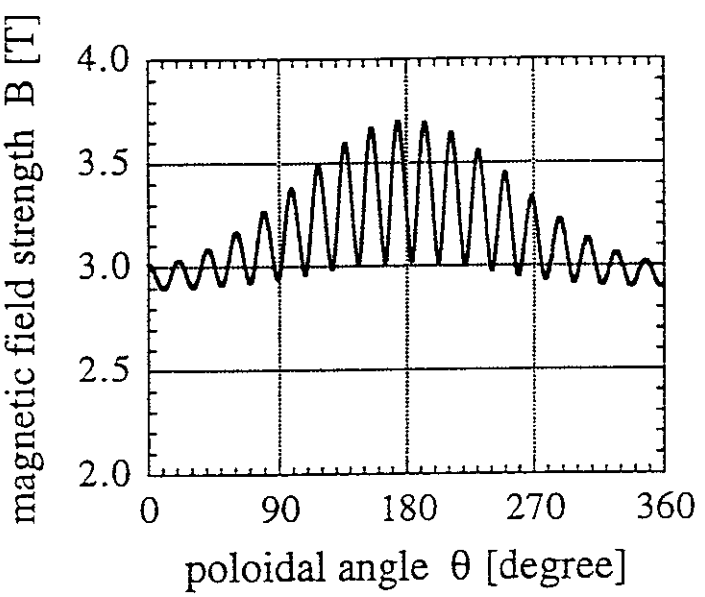
magnetic field strength B [T]
4.0
3.5
3.0
2.5
2.0
0
90
180
270
360
poloidal angle θ [degree]

Fig.3(c)

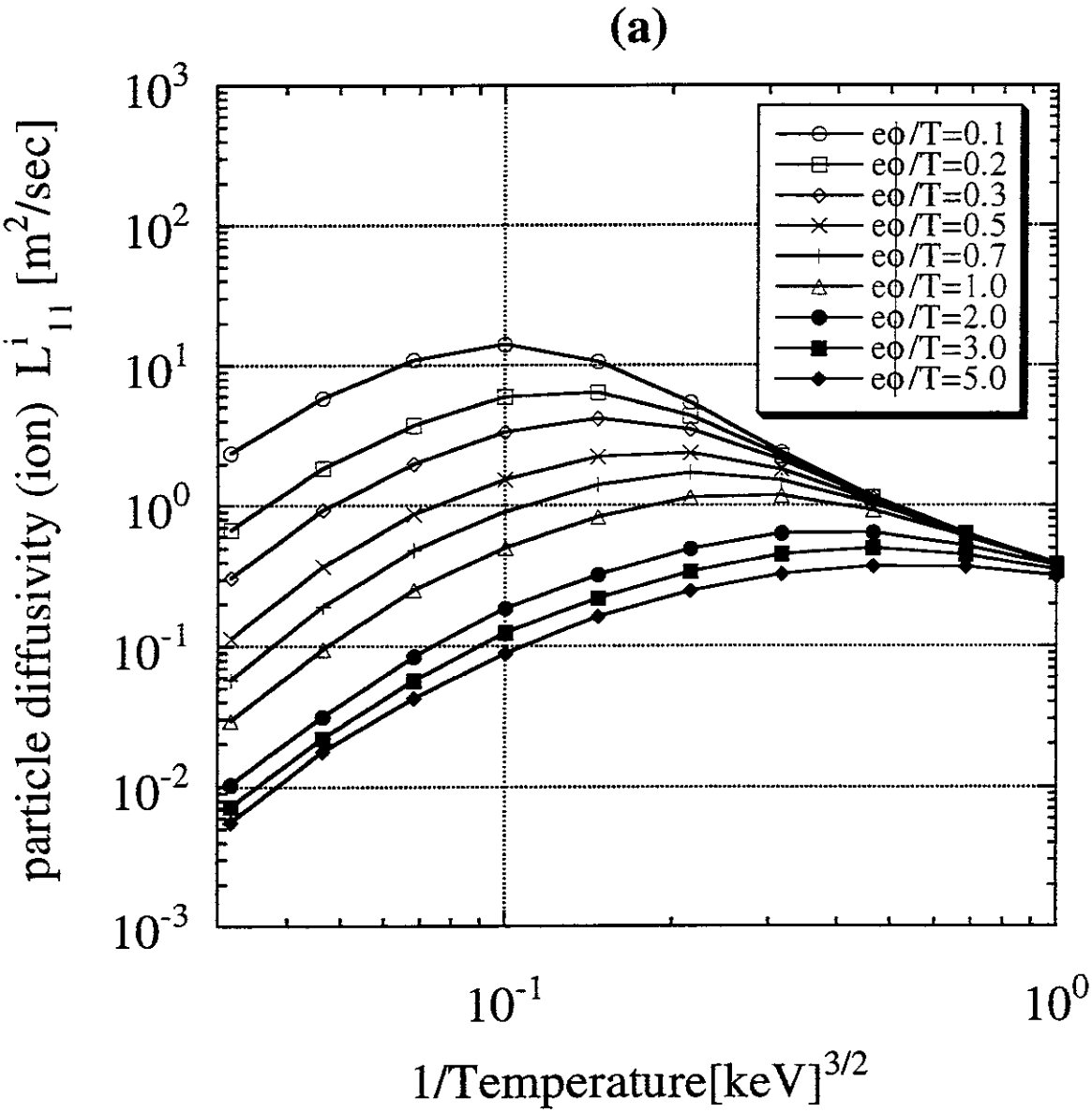
(a)
10^3
10^2
10^1
10^0
10^{-1}
10^{-2}
10^{-3}
particle diffusivity (ion) L^i_{11} [m^2/sec]
eϕ/T=0.1
eϕ/T=0.2
eϕ/T=0.3
eϕ/T=0.5
eϕ/T=0.7
eϕ/T=1.0
eϕ/T=2.0
eϕ/T=3.0
eϕ/T=5.0
10^{-1}
10^0
1/Temperature[keV]$^{3/2}$

Fig.4(a)

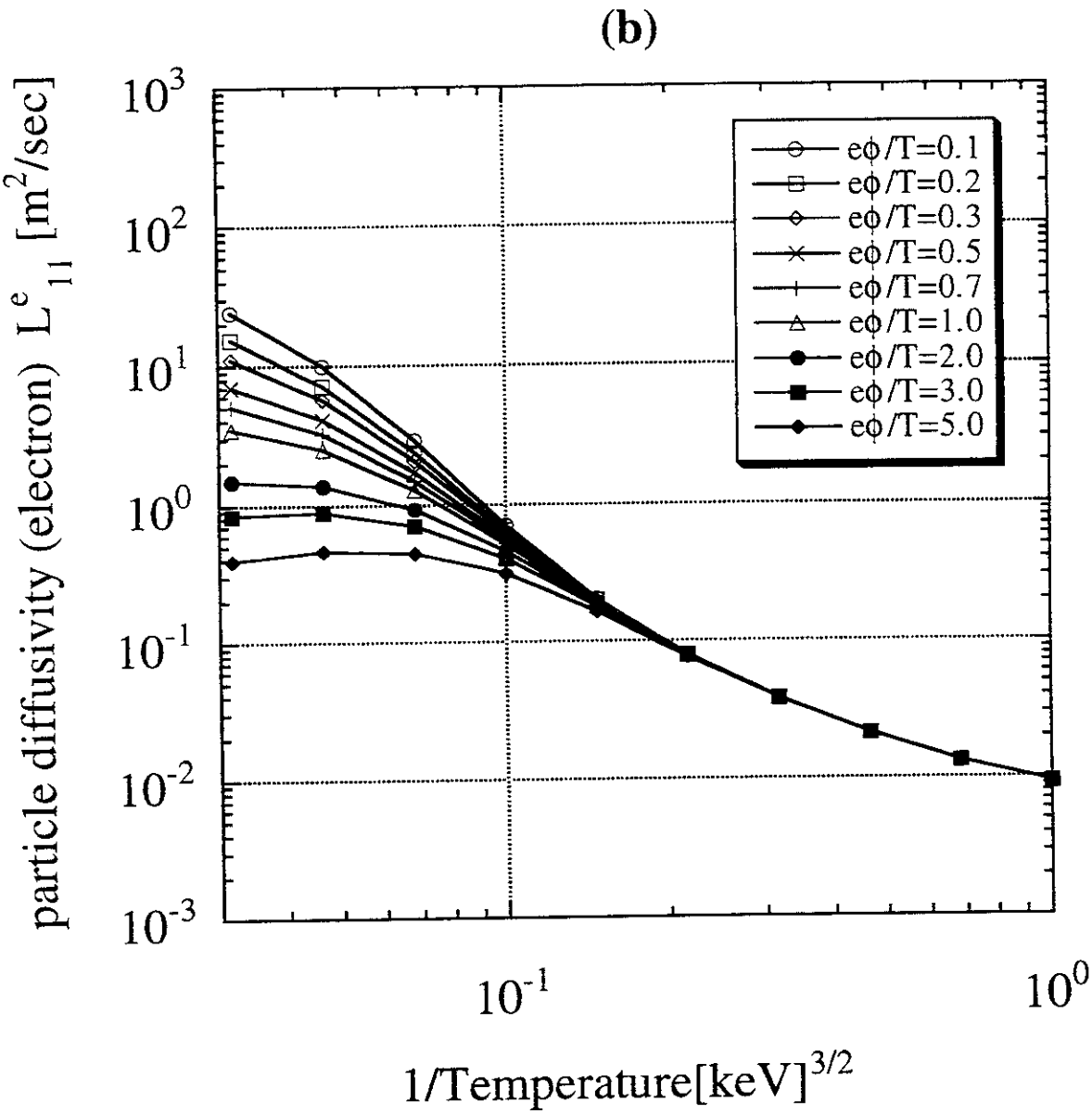
(b)
particle diffusivity (electron) L^e_{11} [m^2/sec]
10^3
10^2
10^1
10^0
10^{-1}
10^{-2}
10^{-3}
eϕ/T=0.1
eϕ/T=0.2
eϕ/T=0.3
eϕ/T=0.5
eϕ/T=0.7
eϕ/T=1.0
eϕ/T=2.0
eϕ/T=3.0
eϕ/T=5.0
10^{-1}
10^0
1/Temperature[keV]$^{3/2}$

Fig.4(b)

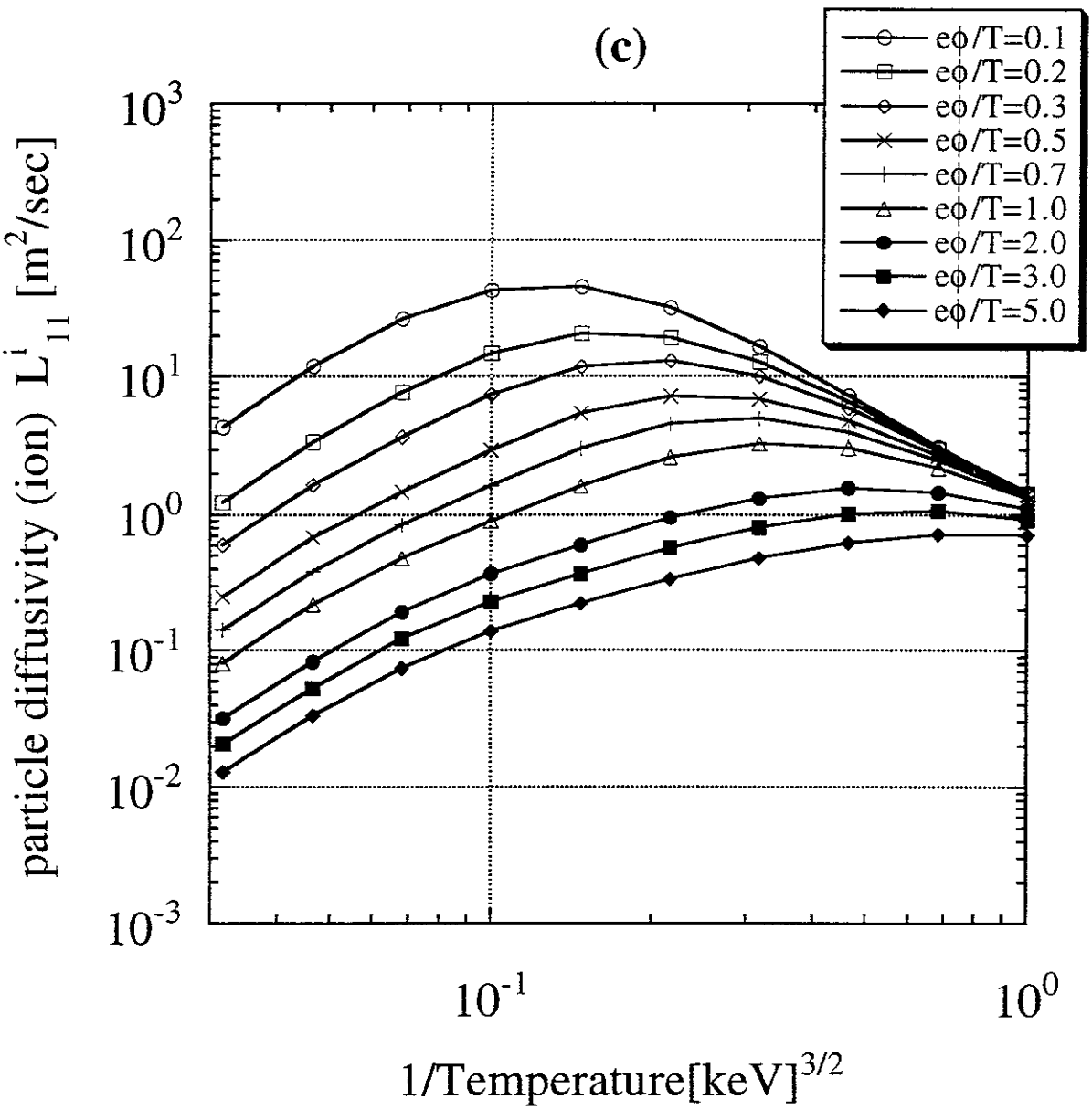
(c)
eϕ/T=0.1
eϕ/T=0.2
eϕ/T=0.3
eϕ/T=0.5
eϕ/T=0.7
eϕ/T=1.0
eϕ/T=2.0
eϕ/T=3.0
eϕ/T=5.0
particle diffusivity (ion) L^i_{11} [m^2/sec]
10^3
10^2
10^1
10^0
10^{-1}
10^{-2}
10^{-3}
10^{-1}
10^0
1/Temperature[keV]$^{3/2}$

Fig.4(c)

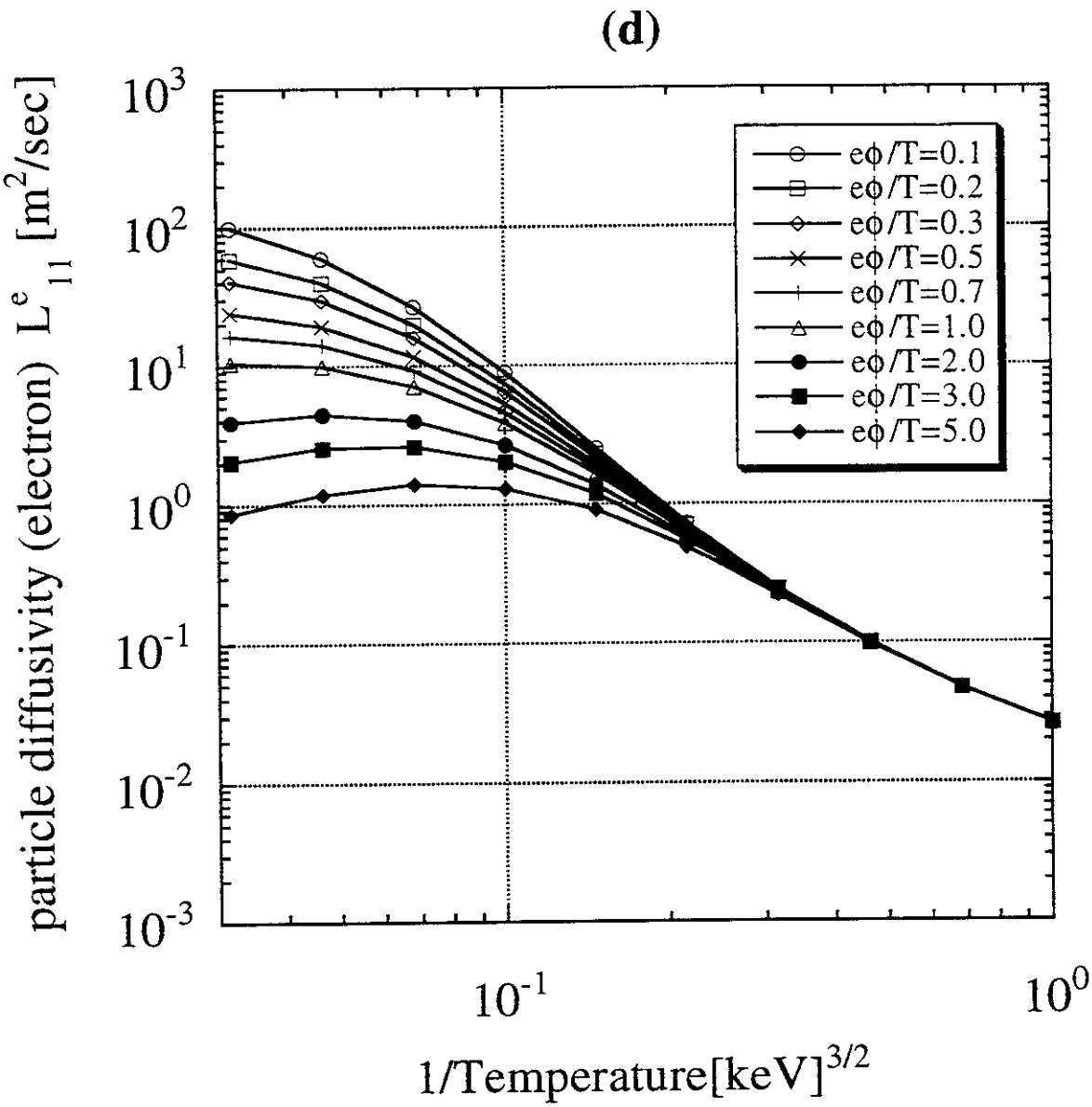
(d)
particle diffusivity (electron) L^e_{11} [m^2/sec]
10^3
10^2
10^1
10^0
10^{-1}
10^{-2}
10^{-3}
eϕ/T=0.1
eϕ/T=0.2
eϕ/T=0.3
eϕ/T=0.5
eϕ/T=0.7
eϕ/T=1.0
eϕ/T=2.0
eϕ/T=3.0
eϕ/T=5.0
10^{-1}
10^0
1/Temperature[keV]$^{3/2}$

Fig.4(d)

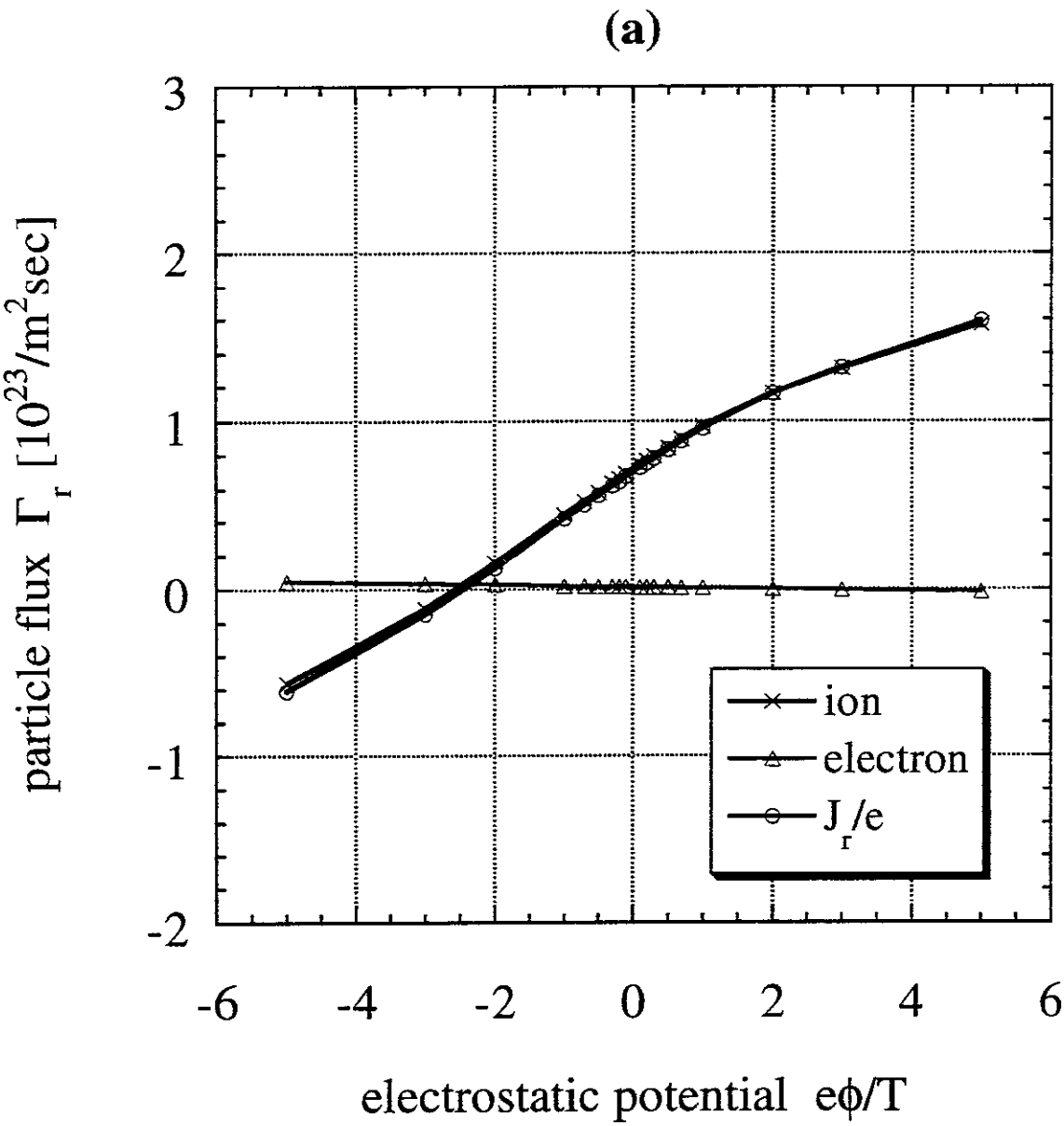
(a)
3
2
1
0
-1
-2
-6
-4
-2
0
2
4
6
particle flux Γ_r [10^{23}/m^{2}sec]
electrostatic potential eϕ/T
ion
electron
J_r/e

Fig.5(a)

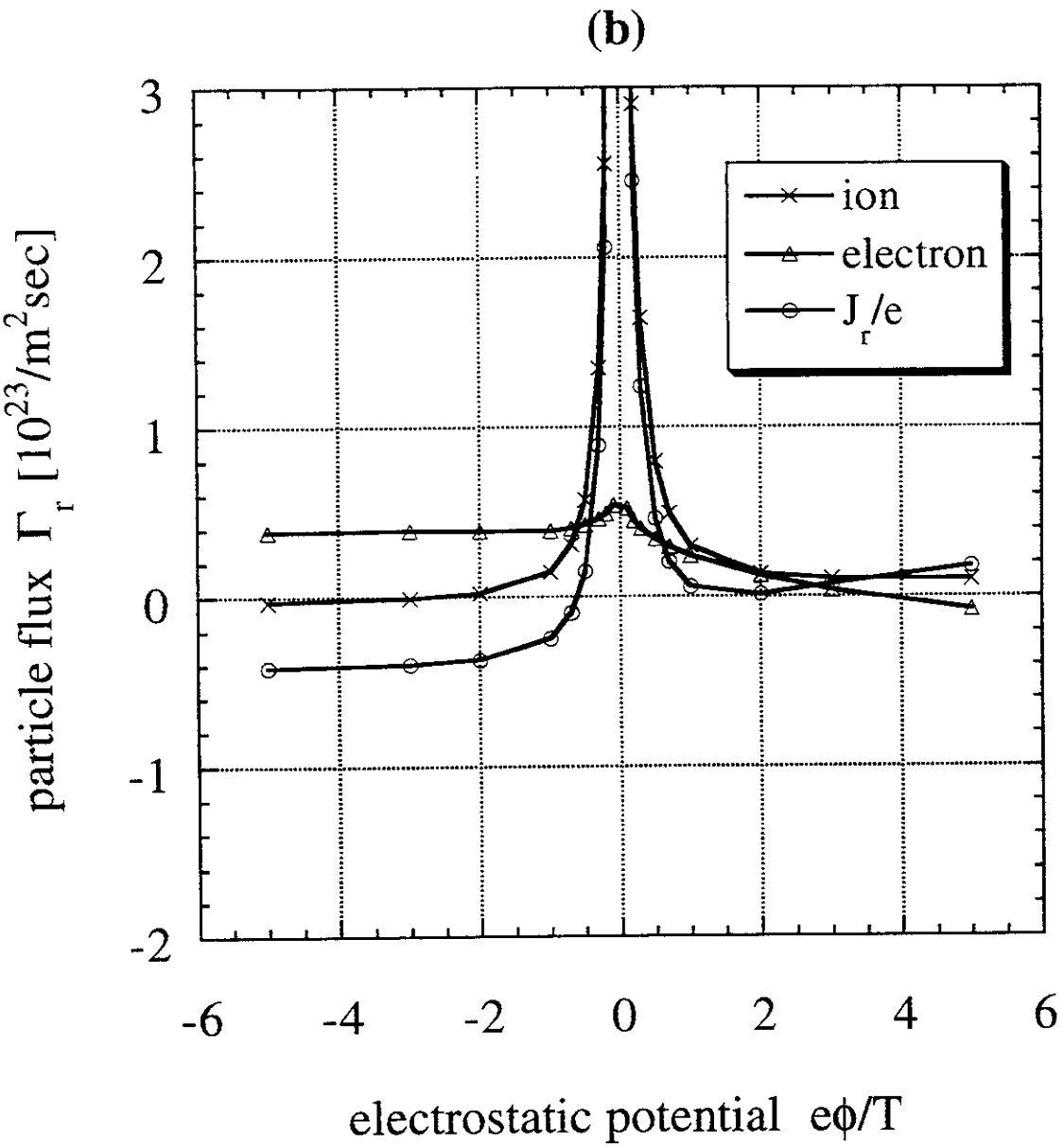
(b)
3
2
1
0
-1
-2
-6
-4
-2
0
2
4
6
ion
electron
J r /e
particle flux Γ r [10^23/m^2sec]
electrostatic potential eϕ/T

Fig.5(b)

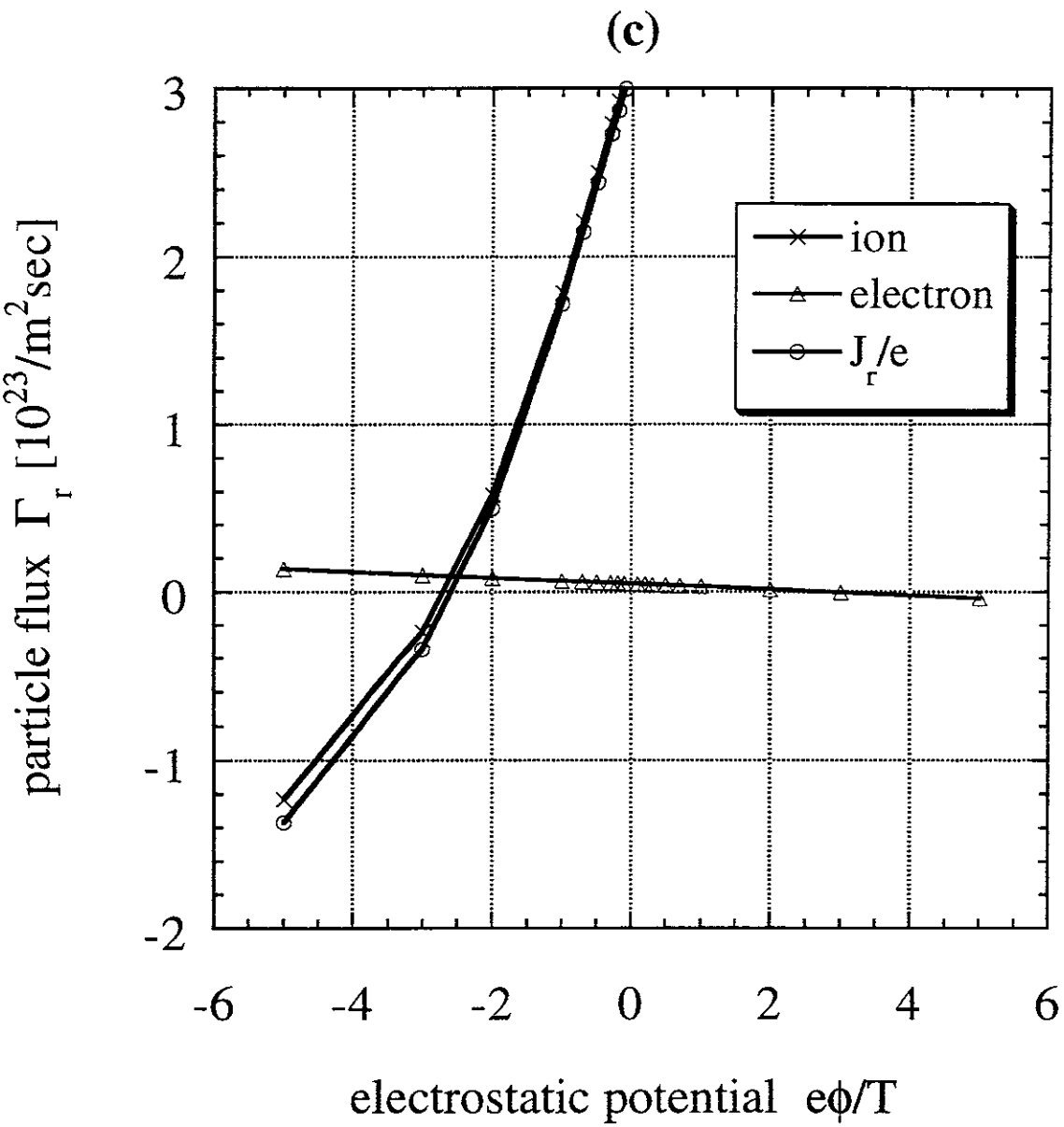
(c)
3
2
1
0
-1
-2
-6
-4
-2
0
2
4
6
ion
electron
J_r/e
particle flux Γ_r [10^23/m^2sec]
electrostatic potential eϕ/T

Fig.5(c)

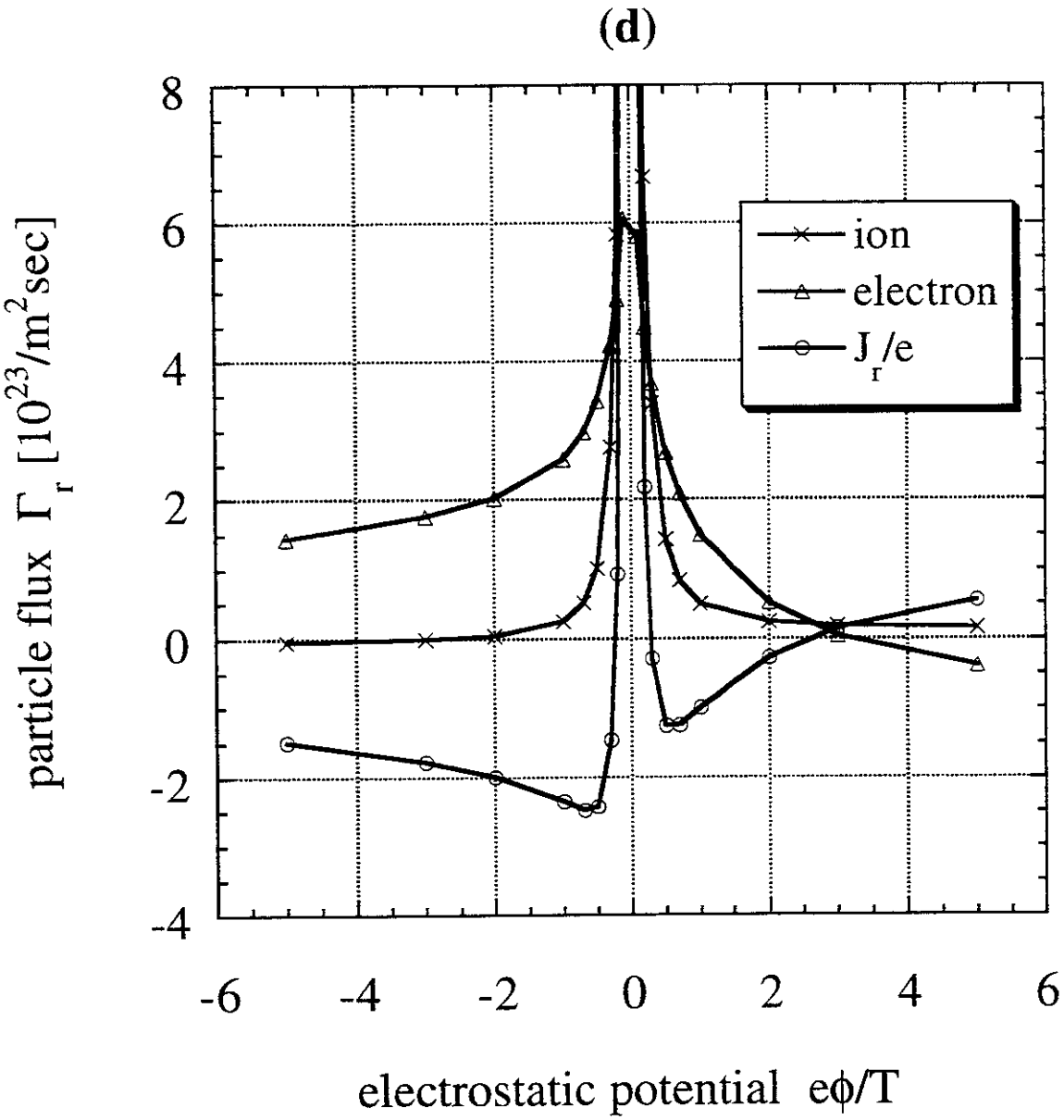
(d)
8
6
4
2
0
-2
-4
-6
-4
-2
0
2
4
6
ion
electron
J r /e
particle flux Γr [10^23/m^2sec]
electrostatic potential eϕ/T

Fig.5(d)

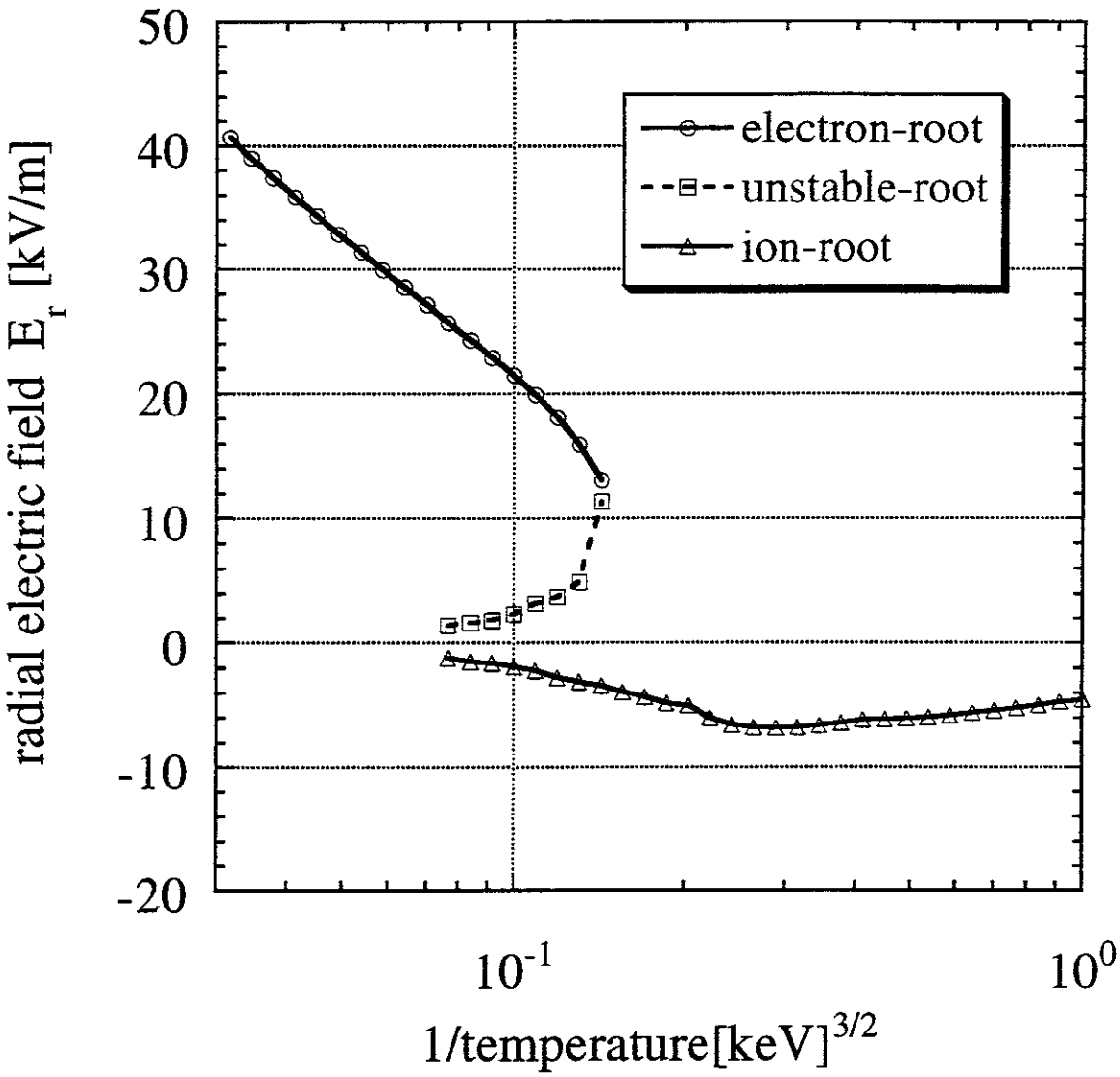
50
40
30
20
10
0
-10
-20
radial electric field E_r [kV/m]
electron-root
unstable-root
ion-root
10^{-1}
10^{0}
1/temperature[keV]$^{3/2}$

Fig.6

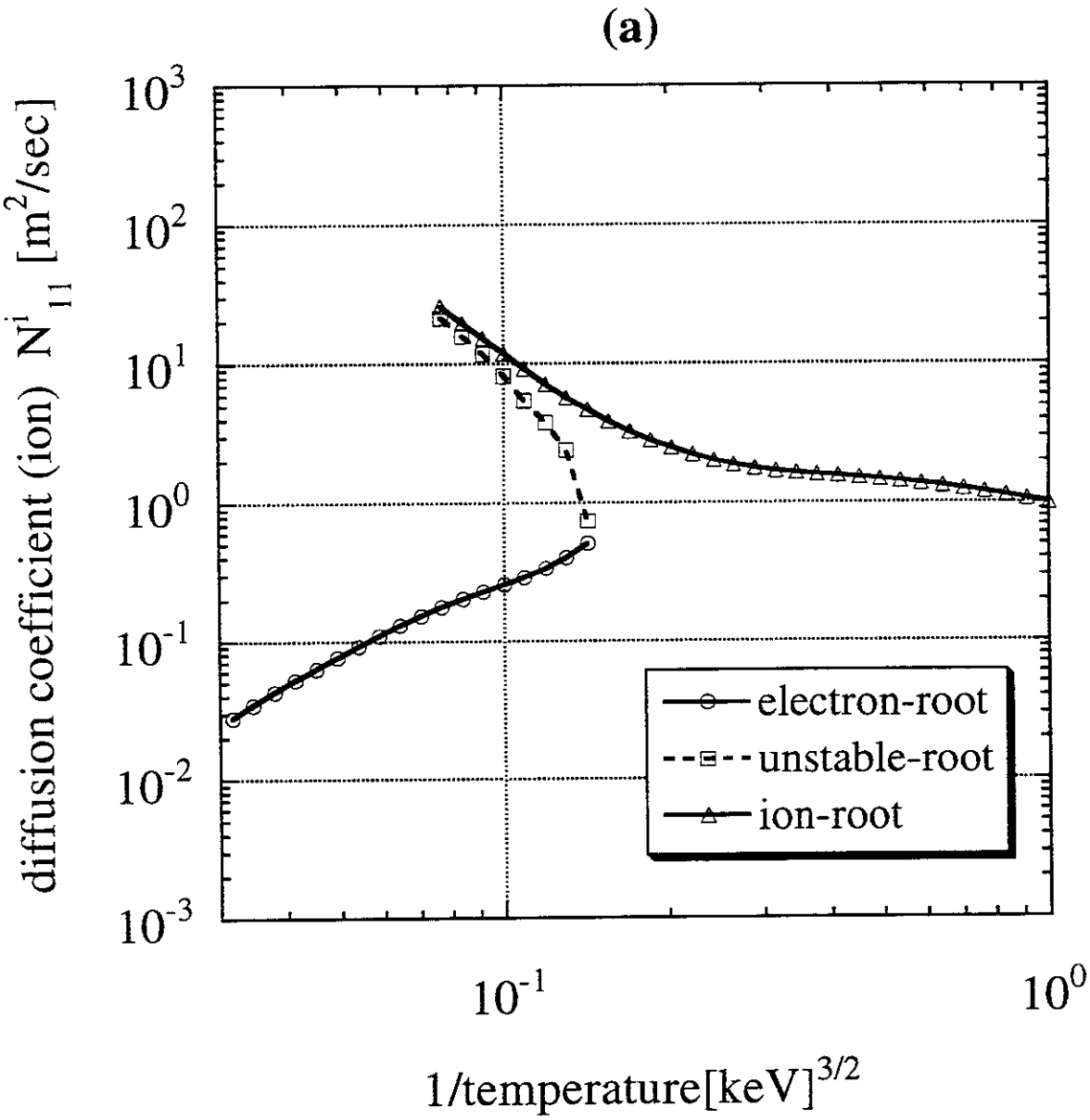
(a)
diffusion coefficient (ion) N^i_{11} [m^2/sec]
10^3
10^2
10^1
10^0
10^{-1}
10^{-2}
10^{-3}
electron-root
unstable-root
ion-root
10^{-1}
10^0
1/temperature[keV]$^{3/2}$

Fig.7(a)

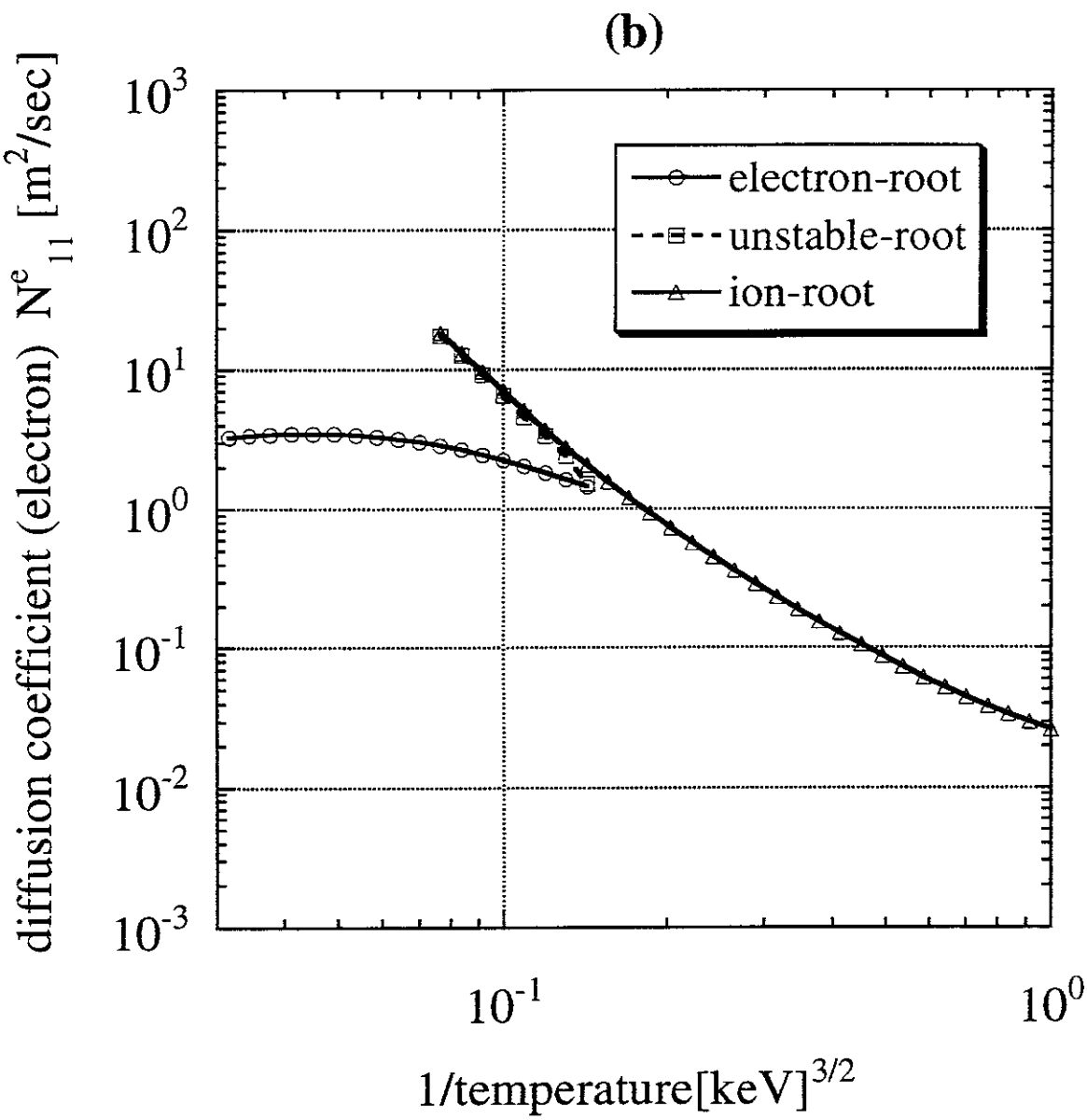
(b)
diffusion coefficient (electron) N^e_{11} [m^2/sec]
10^3
10^2
10^1
10^0
10^{-1}
10^{-2}
10^{-3}
electron-root
unstable-root
ion-root
10^{-1}
10^0
1/temperature[keV]$^{3/2}$

Fig.7(b)

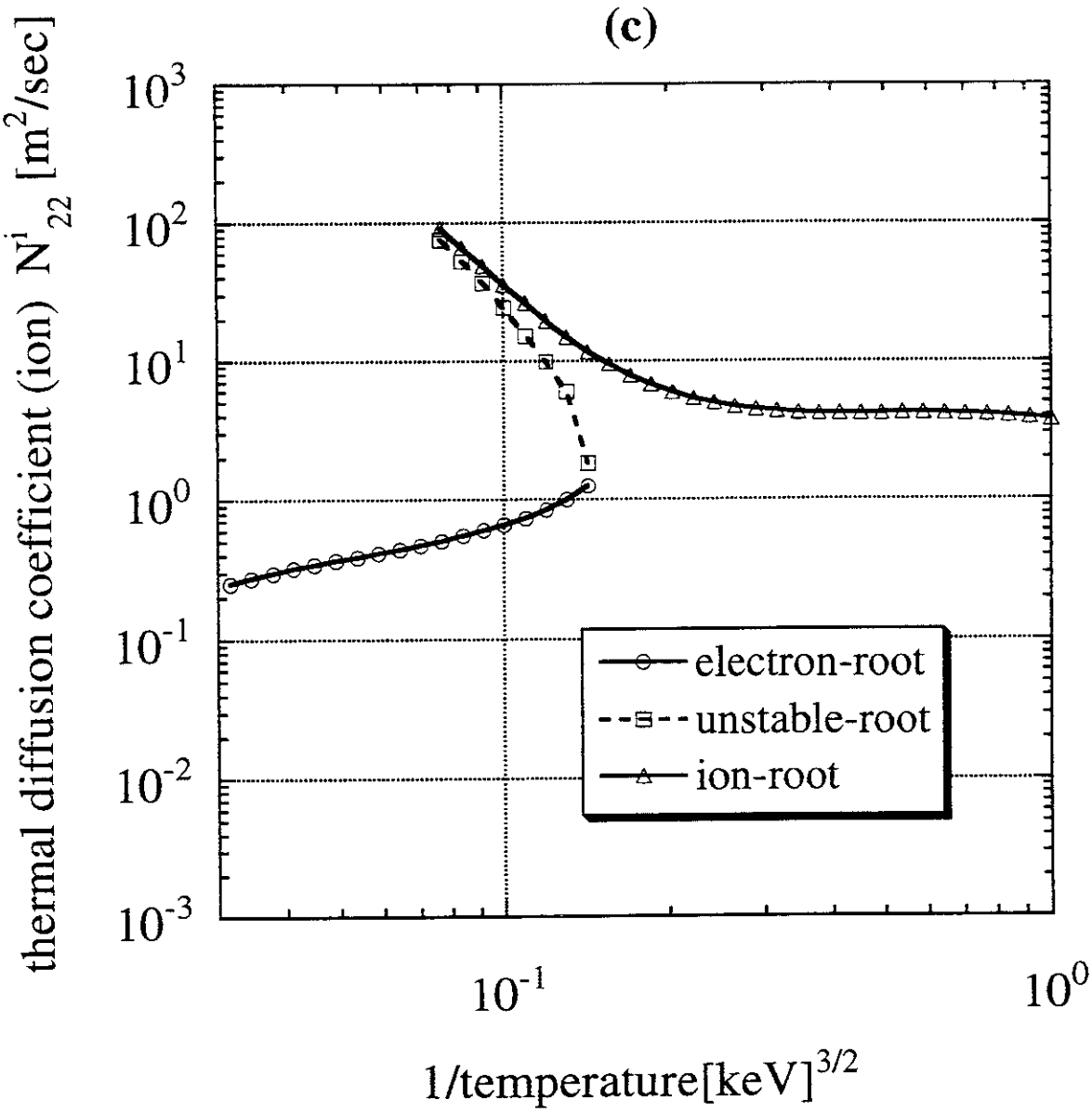
(c)
thermal diffusion coefficient (ion) N^{i}_{22} [m^2/sec]
10^3
10^2
10^1
10^0
10^{-1}
10^{-2}
10^{-3}
electron-root
unstable-root
ion-root
10^{-1}
10^0
1/temperature[keV]$^{3/2}$

Fig.7(c)

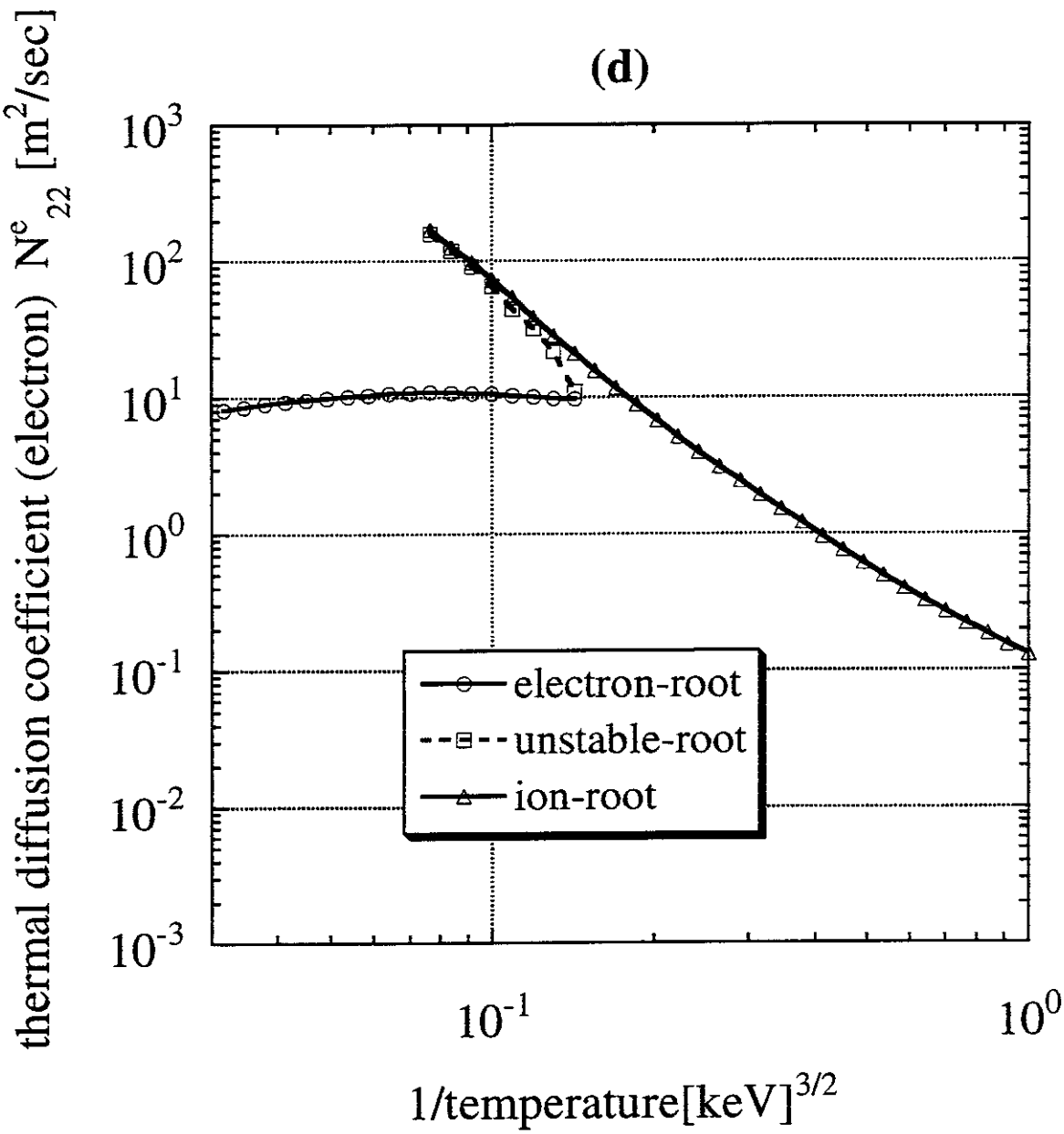
(d)
thermal diffusion coefficient (electron) N^e_{22} [m^2/sec]
10^3
10^2
10^1
10^0
10^{-1}
10^{-2}
10^{-3}
electron-root
unstable-root
ion-root
10^{-1}
10^0
1/temperature[keV]$^{3/2}$

Fig.7(d)

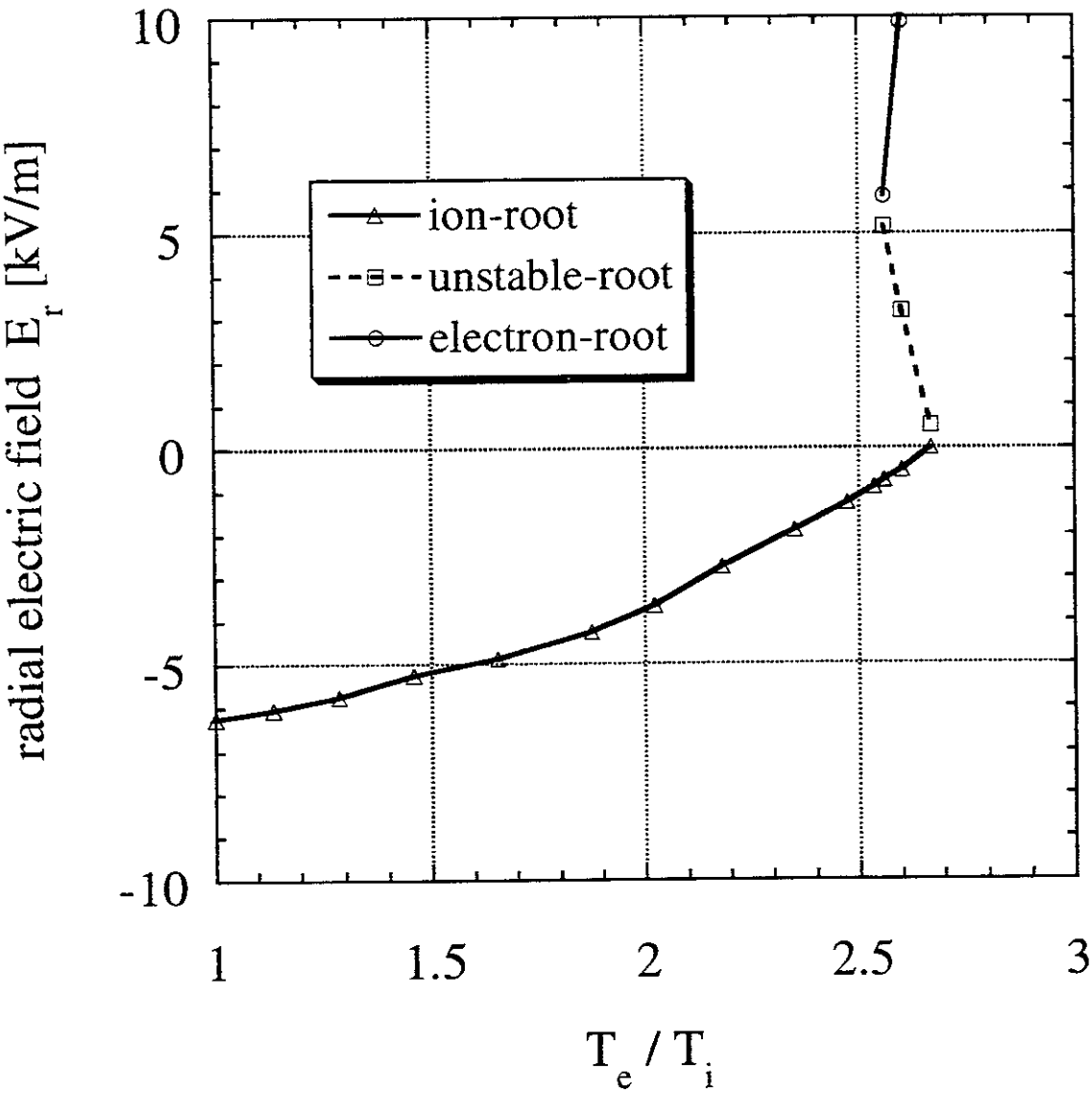
10
5
0
-5
-10
1
1.5
2
2.5
3
radial electric field E_r [kV/m]
T_e / T_i
ion-root
unstable-root
electron-root

Fig.8

TABLE I. ELECTRIC FIELD AND TRANSPORT COEFFICIENTS

TABLE I(a): $\Delta_v = -0.15$ [m], $\beta_0 = 0\%$, $r/a = 0.5$

T [keV]	ϕ [kV]	E_r [kV/m]	N_{11}^i [m^2/s]	N_{22}^i [m^2/s]	N_{11}^e [m^2/s]	N_{22}^e [m^2/s]
1.00	-2.46	-4.45	3.596e-1	1.283	9.264e-3	3.323e-2
4.64	-2.88	-5.22	1.153	3.545	5.597e-1	6.201

TABLE I(b): $\Delta_v = -0.15$ [m], $\beta_0 = 6\%$, $r/a = 0.5$

T [keV]	ϕ [kV]	E_r [kV/m]	N_{11}^i [m^2/s]	N_{22}^i [m^2/s]	N_{11}^e [m^2/s]	N_{22}^e [m^2/s]
1.00	-2.59	-4.50	9.922e-1	3.732	2.638e-2	1.298e-1
4.64	-1.11	-1.92	1.190e+1	3.557e+1	7.019	7.344e+1
4.64	+12.4	+21.4	2.573e-1	6.633e-1	2.254	1.058e+1

TABLE I(c): $\Delta_v = -0.25$ [m], $\beta_0 = 0\%$, $r/a = 0.5$

T [keV]	ϕ [kV]	E_r [kV/m]	N_{11}^i [m^2/s]	N_{22}^i [m^2/s]	N_{11}^e [m^2/s]	N_{22}^e [m^2/s]
1.00	-2.25	-4.06	2.156e-1	6.799e-1	5.899e-3	1.839e-2
4.64	-4.37	-7.90	4.233e-1	1.183	1.760e-1	1.615

TABLE I(d): $\Delta_v = -0.25$ [m], $\beta_0 = 8\%$, $r/a = 0.5$

T [keV]	ϕ [kV]	E_r [kV/m]	N_{11}^i [m^2/s]	N_{22}^i [m^2/s]	N_{11}^e [m^2/s]	N_{22}^e [m^2/s]
1.00	-2.43	-4.14	9.911e-1	3.550	2.677e-2	1.093e-1
4.64	-1.94	-3.30	6.423	2.040e+1	3.630	4.016e+1
4.64	+13.1	+22.3	2.105e-1	4.391e-1	1.778	1.008e+1

TABLE II. ELECTRIC FIELD AND TRANSPORT COEFFICIENTS FOR $T_i \approx 2\ T_e$

TABLE II(a): $\Delta_v = -0.15$ [m], $\beta_0 = 6\%$, $r/a = 0.5$

T_i [keV]	T_e [keV]	ϕ [kV]	E_r [kV/m]	N^i_{11} [m^2/s]	N^i_{22} [m^2/s]	N^e_{11} [m^2/s]	N^e_{22} [m^2/s]
4.64	2.15	-7.08	-12.3	7.574e-1	2.187	1.851e-1	1.051

TABLE II(b): $\Delta_v = -0.25$ [m], $\beta_0 = 8\%$, $r/a = 0.5$

T_i [keV]	T_e [keV]	ϕ [kV]	E_r [kV/m]	N^i_{11} [m^2/s]	N^i_{22} [m^2/s]	N^e_{11} [m^2/s]	N^e_{22} [m^2/s]
4.64	2.15	-7.94	-13.5	6.486e-1	1.929	1.429e-1	7.596e-1

Recent Issues of NIFS Series

NIFS-433 R. Horiuchi and T. Sato,
Particle Simulation Study of Collisionless Driven Reconnection in a Sheared Magnetic Field; Aug. 1996

NIFS-434 Y. Suzuki, K. Kusano and K. Nishikawa,
Three-Dimensional Simulation Study of the Magnetohydrodynamic Relaxation Process in the Solar Corona. II.; Aug. 1996

NIFS-435 H. Sugama and W. Horton,
Transport Processes and Entropy Production in Toroidally Rotating Plasmas with Electrostatic Turbulence; Aug. 1996

NIFS-436 T. Kato, E. Rachlew-Källne, P. Hörling and K.-D Zastrow,
Observations and Modelling of Line Intensity Ratios of OV Multiplet Lines for 2s3s 3S1 - 2s3p 3Pj; Aug. 1996

NIFS-437 T. Morisaki, A. Komori, R. Akiyama, H. Idei, H. Iguchi, N. Inoue, Y. Kawai, S. Kubo, S. Masuzaki, K. Matsuoka, T. Minami, S. Morita, N. Noda, N. Ohyabu, S. Okamura, M. Osakabe, H. Suzuki, K. Tanaka, C. Takahashi, H. Yamada, I. Yamada and O. Motojima,
Experimental Study of Edge Plasma Structure in Various Discharges on Compact Helical System; Aug. 1996

NIFS-438 A. Komori, N. Ohyabu, S. Masuzaki, T. Morisaki, H. Suzuki, C. Takahashi, S. Sakakibara, K. Watanabe, T. Watanabe, T. Minami, S. Morita, K. Tanaka, S. Ohdachi, S. Kubo, N. Inoue, H. Yamada, K. Nishimura, S. Okamura, K. Matsuoka, O. Motojima, M. Fujiwara, A. Iiyoshi, C. C. Klepper, J.F. Lyon, A.C. England, D.E. Greenwood, D.K. Lee, D.R. Overbey, J.A. Rome, D.E. Schechter and C.T. Wilson,
Edge Plasma Control by a Local Island Divertor in the Compact Helical System; Sep. 1996 (IAEA-CN-64/C1-2)

NIFS-439 K. Ida, K. Kondo, K. Nagaski T. Hamada, H. Zushi, S. Hidekuma, F. Sano, T. Mizuuchi, H. Okada, S. Besshou, H. Funaba, Y. Kurimoto, K. Watanabe and T. Obiki,
Dynamics of Ion Temperature in Heliotron-E; Sep. 1996 (IAEA-CN-64/CP-5)

NIFS-440 S. Morita, H. Idei, H. Iguchi, S. Kubo, K. Matsuoka, T. Minami, S. Okamura, T. Ozaki, K. Tanaka, K. Toi, R. Akiyama, A. Ejiri, A. Fujisawa, M. Fujiwara, M. Goto, K. Ida, N. Inoue, A. Komori, R. Kumazawa, S. Masuzaki, T. Morisaki, S. Muto, K. Narihara, K. Nishimura, I. Nomura, S. Ohdachi, M.. Osakabe, A. Sagara, Y. Shirai, H. Suzuki, C. Takahashi, K. Tsumori, T. Watari, H. Yamada and I. Yamada,
A Study on Density Profile and Density Limit of NBI Plasmas in CHS; Sep. 1996 (IAEA-CN-64/CP-3)

NIFS-441 O. Kaneko, Y. Takeiri, K. Tsumori, Y. Oka, M. Osakabe, R. Akiyama, T.

Kawamoto, E. Asano and T. Kuroda,
Development of Negative-Ion-Based Neutral Beam Injector for the Large Helical Device; Sep. 1996 (IAEA-CN-64/GP-9)

NIFS-442 K. Toi, K.N. Sato, Y. Hamada, S. Ohdachi, H. Sakakita, A. Nishizawa, A. Ejiri, K. Narihara, H. Kuramoto, Y. Kawasumi, S. Kubo, T. Seki, K. Kitachi, J. Xu, K. Ida, K. Kawahata, I. Nomura, K. Adachi, R. Akiyama, A. Fujisawa, J. Fujita, N. Hiraki, S. Hidekuma, S. Hirokura, H. Idei, T. Ido, H. Iguchi, K. Iwasaki, M. Isobe, O. Kaneko, Y. Kano, M. Kojima, J. Koog, R. Kumazawa, T. Kuroda, J. Li, R. Liang, T. Minami, S. Morita, K. Ohkubo, Y. Oka, S. Okajima, M. Osakabe, Y. Sakawa, M. Sasao, K. Sato, T. Shimpo, T. Shoji, H. Sugai, T. Watari, I. Yamada and K. Yamauti,
Studies of Perturbative Plasma Transport, Ice Pellet Ablation and Sawtooth Phenomena in the JIPP T-IIU Tokamak; Sep. 1996 (IAEA-CN-64/A6-5)

NIFS-443 Y. Todo, T. Sato and The Complexity Simulation Group,
Vlasov-MHD and Particle-MHD Simulations of the Toroidal Alfvén Eigenmode; Sep. 1996 (IAEA-CN-64/D2-3)

NIFS-444 A. Fujisawa, S. Kubo, H. Iguchi, H. Idei, T. Minami, H. Sanuki, K. Itoh, S. Okamura, K. Matsuoka, K. Tanaka, S. Lee, M. Kojima, T.P. Crowley, Y. Hamada, M. Iwase, H. Nagasaki, H. Suzuki, N. Inoue, R. Akiyama, M. Osakabe, S. Morita, C. Takahashi, S. Muto, A. Ejiri, K. Ida, S. Nishimura, K. Narihara, I. Yamada, K. Toi, S. Ohdachi, T. Ozaki, A. Komori, K. Nishimura, S. Hidekuma, K. Ohkubo, D.A. Rasmussen, J.B. Wilgen, M. Murakami, T. Watari and M. Fujiwara,
An Experimental Study of Plasma Confinement and Heating Efficiency through the Potential Profile Measurements with a Heavy Ion Beam Probe in the Compact Helical System; Sep. 1996 (IAEA-CN-64/C1-5)

NIFS-445 O. Motojima, N. Yanagi, S. Imagawa, K. Takahata, S. Yamada, A. Iwamoto, H. Chikaraishi, S. Kitagawa, R. Maekawa, S. Masuzaki, T. Mito, T. Morisaki, A. Nishimura, S. Sakakibara, S. Satoh, T. Satow, H. Tamura, S. Tanahashi, K. Watanabe, S. Yamaguchi, J. Yamamoto, M.Fujiwara and A. Iiyoshi,
Superconducting Magnet Design and Construction of LHD; Sep. 1996 (IAEA-CN-64/G2-4)

NIFS-446 S. Murakami, N. Nakajima, S. Okamura, M. Okamoto and U. Gasparino,
Orbit Effects of Energetic Particles on the Reachable β–Value and the Radial Electric Field in NBI and ECR Heated Heliotron Plasmas; Sep. 1996 (IAEA-CN-64/CP -6) Sep. 1996

NIFS-447 K. Yamazaki, A. Sagara, O. Motojima, M. Fujiwara, T. Amano, H. Chikaraishi, S. Imagawa, T. Muroga, N. Noda, N. Ohyabu, T. Satow, J.F. Wang, K.Y. Watanabe, J. Yamamoto , H. Yamanishi, A. Kohyama, H. Matsui, O. Mitarai, T. Noda, A.A. Shishkin, S. Tanaka and T. Terai
Design Assessment of Heliotron Reactor; Sep. 1996 (IAEA-CN-64/G1-5)

NIFS-448 M. Ozaki, T. Sato and the Complexity Simulation Group,
Interactions of Convecting Magnetic Loops and Arcades; Sep. 1996

NIFS-449 T. Aoki,
Interpolated Differential Operator (IDO) Scheme for Solving Partial Differential Equations; Sep. 1996

NIFS-450 D. Biskamp and T. Sato,
Partial Reconnection in the Sawtooth Collapse; Sep. 1996

NIFS-451 J. Li, X. Gong, L. Luo, F.X. Yin, N. Noda, B. Wan, W. Xu, X. Gao, F. Yin, J.G. Jiang, Z. Wu., J.Y. Zhao, M. Wu, S. Liu and Y. Han,
Effects of High Z Probe on Plasma Behavior in HT-6M Tokamak; Sep. 1996

NIFS-452 N. Nakajima, K. Ichiguchi, M. Okamoto and R.L. Dewar,
Ballooning Modes in Heliotrons/Torsatrons; Sep. 1996 (IAEA-CN-64/D3-6)

NIFS-453 A. Iiyoshi,
Overview of Helical Systems; Sep. 1996 (IAEA-CN-64/O1-7)

NIFS-454 S. Saito, Y. Nomura, K. Hirose and Y.H. Ichikawa,
Separatrix Reconnection and Periodic Orbit Annihilation in the Harper Map; Oct. 1996

NIFS-455 K. Ichiguchi, N. Nakajima and M. Okamoto,
Topics on MHD Equilibrium and Stability in Heliotron / Torsatron; Oct. 1996

NIFS-456 G. Kawahara, S. Kida, M. Tanaka and S. Yanase,
Wrap, Tilt and Stretch of Vorticity Lines around a Strong Straight Vortex Tube in a Simple Shear Flow; Oct. 1996

NIFS-457 K. Itoh, S.- I. Itoh, A. Fukuyama and M. Yagi,
Turbulent Transport and Structural Transition in Confined Plasmas; Oct. 1996

NIFS-458 A. Kageyama and T. Sato,
Generation Mechanism of a Dipole Field by a Magnetohydrodynamic Dynamo; Oct. 1996

NIFS-459 K. Araki, J. Mizushima and S. Yanase,
The Non-axisymmetric Instability of the Wide-Gap Spherical Couette Flow; Oct. 1996

NIFS-460 Y. Hamada, A. Fujisawa, H. Iguchi, A. Nishizawa and Y. Kawasumi,
A Tandem Parallel Plate Analyzer; Nov. 1996

NIFS-461 Y. Hamada, A. Nishizawa, Y. Kawasumi, A. Fujisawa, K. Narihara, K. Ida, A. Ejiri, S. Ohdachi, K. Kawahata, K. Toi, K. Sato, T. Seki, H. Iguchi, K. Adachi, S. Hidekuma, S.Hirokura, K. Iwasaki, T. Ido, M. Kojima, J. Koong, R. Kumazawa, H. Kuramoto, T. Minami, I. Nomura, H. Sakakita, M. Sasao, K.N. Sato, T. Tsuzuki, J. Xu, I. Yamada and T. Watari,

Density Fluctuation in JIPP T-IIU Tokamak Plasmas Measured by a Heavy Ion Beam Probe; Nov. 1996

NIFS-462 N. Katsuragawa, H. Hojo and A. Mase,
Simulation Study on Cross Polarization Scattering of Ultrashort-Pulse Electromagnetic Waves; Nov. 1996

NIFS-463 V. Voitsenya, V. Konovalov, O. Motojima, K. Narihara, M. Becker and B. Schunke,
Evaluations of Different Metals for Manufacturing Mirrors of Thomson Scattering System for the LHD Divertor Plasma; Nov. 1996

NIFS-464 M. Pereyaslavets, M. Sato, T. Shimozuma, Y. Takita, H. Idei, S. Kubo, K. Ohkubo and K. Hayashi,
Development and Simulation of RF Components for High Power Millimeter Wave Gyrotrons; Nov. 1997

NIFS-465 V.S. Voitsenya, S. Masuzaki, O. Motojima, N. Noda and N. Ohyabu,
On the Use of CX Atom Analyzer for Study Characteristics of Ion Component in a LHD Divertor Plasma; Dec. 1996

NIFS-466 H. Miura and S. Kida,
Identification of Tubular Vortices in Complex Flows; Dec. 1996

NIFS-467 Y. Takeiri, Y. Oka, M. Osakabe, K. Tsumori, O. Kaneko, T. Takanashi, E. Asano, T. Kawamoto, R. Akiyama and T. Kuroda,
Suppression of Accelerated Electrons in a High-current Large Negative Ion Source; Dec. 1996

NIFS-468 A. Sagara, Y. Hasegawa, K. Tsuzuki, N. Inoue, H. Suzuki, T. Morisaki, N. Noda, O. Motojima, S. Okamura, K. Matsuoka, R. Akiyama, K. Ida, H. Idei, K. Iwasaki, S. Kubo, T. Minami, S. Morita, K. Narihara, T. Ozaki, K. Sato, C. Takahashi, K. Tanaka, K. Toi and I. Yamada,
Real Time Boronization Experiments in CHS and Scaling for LHD; Dec. 1996

NIFS-469 V.L. Vdovin, T.Watari and A. Fukuyama,
3D Maxwell-Vlasov Boundary Value Problem Solution in Stellarator Geometry in Ion Cyclotron Frequency Range (final report); Dec. 1996

NIFS-470 N. Nakajima, M. Yokoyama, M. Okamoto and J. Nührenberg,
Optimization of M=2 Stellarator; Dec. 1996

NIFS-471 A. Fujisawa, H. Iguchi, S. Lee and Y. Hamada,
Effects of Horizontal Injection Angle Displacements on Energy Measurements with Parallel Plate Energy Analyzer; Dec. 1996

NIFS-472 R. Kanno, N. Nakajima, H. Sugama, M. Okamoto and Y. Ogawa,
Effects of Finite-β and Radial Electric Fields on Neoclassical Transport in the Large Helical Device; Jan. 1997